Coupled Electro-Thermal Model for Submarine HVDC Power Cables

Master of Science Thesis in Electric Power Engineering

MATTEWOS BERHANE TEFFERI

Department of Materials and Manufacturing Technology
Division of High Voltage Engineering
CHALMERS UNIVERSITY OF TECHNOLOGY
Göteborg, Sweden, 2013
Report No. 109/2013

Coupled Electro-Thermal Model for Submarine HVDC Power Cables

by

MATTEWOS BERHANE TEFFERI

Diploma work number 109/2013
Division of High Voltage Engineering
Department of Materials and Manufacturing Technology
CHALMERS UNIVERSITY OF TECHNOLOGY
Gothenburg, Sweden 2013

Diploma work in the Master program on ELECTRIC POWER ENGINEERING

Performed at: Nexans Norway AS
Knivsøvn.70, P.O.Box 41
NO-1751
Halden, Norway

Supervisors: Ramona Huuva, Lic Eng
Project Engineer- Extruded HVDC Submarine High Voltage Cables

Marius Hatlo, PhD
Specialist Engineer Technological Analysis Center Hybrid Underwater Cables Business Line

Examiner: Yuriy Serdyuk, Associate Professor
High Voltage Engineering
Department of Materials and Manufacturing Technology
Chalmers University of Technology
SE-412 96 Gothenburg, Sweden

Coupled Electro-Thermal Model for Submarine HVDC Power Cables
MATTEWOS BERHANE TEFFERI

Diploma work no 109/2013
Division of High Voltage Engineering
Department of Materials and Manufacturing Technology
Chalmers University of Technology
SE-412 96 Gothenburg, Sweden
Telephone + 46 (0)31-772 1000

Chalmers Reproservice
Gothenburg, 2013

Coupled Electro-Thermal Model for Submarine HVDC Power Cables

MATTEWOS BERHANE TEFFERI

Division of High Voltage Engineering
Department of Materials and Manufacturing Technology
Chalmers University of Technology

Abstract

HVDC cables have a significant role in linking power grids and therefore recent development of HVDC cables with polymeric insulation has received much attention. Unlike HVAC cables, the electric field across the insulation of extruded HVDC cables is affected by the conductivity of the material, which is a function of both the electric field and temperature. The focus of this thesis is on calculations of coupled electrical and thermal nonlinear transient processes in cable insulation and their effects on the internal electric stresses.

A computer program has been developed in MATLAB for numerical study of the transient nonlinear coupled problem. The program uses finite volume space discretization and Crank-Nicolson time stepping scheme. The developed computational tool takes into account a coupling between the electric field distribution and the thermal effect across cable insulation.

Index Terms: solid dielectrics, finite volume method (FVM), coupled problem, submarine cables, HVDC system, space charge, temperature gradient.

To my Mother

The fear of GOD is the beginning of wisdom.

Psalm 111:10

Acknowledgment

First, I would like to express my sincere appreciation to my supervisor Ramona Huuva for the opportunity she has given me to take this master thesis and for her advice and support throughout my thesis study.

I wish to express my sincere gratitude and appreciation to Marius Halto for his invaluable advices, supervision, encouragement help and patience during the work especially on the numerical modeling, Without him this work would not be possible. Thanks Björn Sonerud for the nice discussions and inputs through the work.

I warmly thank all colleagues at the TAS, Nexans for providing a friendly and stimulating work environment. In particular, I would like to thank Øivind Bergene for making the working environment as much a fun place as possible.

I would also like to thank my examiner Yuriy Serdyuk for reviewing the thesis and for his continuous follow up.

Thanks Jonas Nøland for helping me with my stay in Norway and with my study at Chalmers. Thank you very much for your effort to make the best of conditions when things get frustrating. I would like also to thank Tigist Mebrahtu for you kind help in my stay at Gothenburg.

My special thanks go to the Swedish International Development Cooperation Agency (SIDA) for sponsoring my master study.

Lastly, the most important peoples in my life are my family. My late mother Tsehaynesh G. Medhin, my father Berhane Tefferi, my elder brothers and sisters for being extremely supportive and understanding throughout my studies.

Mom, I love and miss you very much and still think about you to this day. I only hope you are proud of your son, who is doing his best in life and keeps your memory alive.

Mattewos Berhane

Halden, June 2013

Contents

List of Symbols

Directional Derivatives

∇	Gradient
$\nabla \cdot$	Divergence

Constants

k_B	$= 1.38 \times 10^{-23}\ [J/K]$	Boltzmann constant
q	$= 1.60 \times 10^{-19}\ [C]$	Elementary charge
δ	$= 5.6703 \times 10^{-8}\ [W/m^2K^4]$	Stefan-Boltzmann constant
ε_o	$= 8.85 \times 10^{-12}\ [F/m]$	Permittivity of free space

Parameters

A	Area $[m^2]$
C_p	Heat capacity $[J/kgK]$
E	Electric field $[V/m]$
h	Convection heat transfer coefficient $[W/m^2 \cdot K]$
J	the current density $[A/m]$
k	Thermal conductivity $[W/m \cdot K]$
Q	Heat flux $[W]$
r	Radial position $[m]$
S_{heat}	Resistive loss in the insulation $[W]$
t	time[s]

Δt	Finite time[s]
T	Temperature [*K*]
T_s	Surface temperature [*K*]
T_∞	Ambient temperature [*K*]
U	Electric potential [*V*]
α	Temperature dependent coefficient
ε_r	Relative permitivity [*As/Vm*]
ρ_m	Mass density [kg/m^3]
ε	Emissivity
σ_0	Conductivity at 0 ℃ and 0 *V/m*
σ	Conductivity [*S/m*]
γ	Electric field dependent coefficient
ρ	Space charge [*C*]
ϕ	Thermal activation energy [*eV*]

List of Abbreviations

℃	Degrees Celsius
2D	Two Dimensional
AC	Alternating Current
DC	Direct Current
FVM	Finite Volume Methode
HVDC	High Voltage Direct Current
HVAC	High Voltage Alternative Current
MI	Mass Impregnated
MI-PPL	Mass Impregnated Paper Polypropylene Laminate
RC	Resistance - Capacitance
SCFF	Self-Contained Fluid Filled
XLPE	Cross Linked Polyethylene

Chapter 1

Introduction

This chapter answers: "why this study has been made?"

1.1 Background

Electric power systems have a long and varied history beginning more than one hundred years ago. The first commercial electricity generated by Thomas Edison was a direct current (DC) power. Residential areas and neighboring establishments were supplied by short DC lines. However, DC power at low voltage could not be transmitted over long distances, thus stimulated a development of high voltage alternating current (AC) systems. At the end of the 19th century, an AC power transmission has been introduced to transmit power from power generation plants to customers. The development and expansion of AC systems over many decades resulted in a fast growth in power demand. However, the advantages of AC interconnection systems weakened due to technical co-ordination problems. In addition, development of high voltage valves enables DC power to be transmitted at high voltages and over long distances. Furthermore, the practical feasibility of HVDC system is their ability to interconnect bulk power transmissions under water. This makes submarine power cables to be the most significant element in HVDC transmissions [1].

The use of extruded polymers as insulation material in HVDC power cables has the advantage of relatively low cost and good environmental performance. However, the design of extruded power cables is complex, since the electric field distribution in a DC cable is mainly governed by the conductivity, which is dependent on both the electric field and temperature [2]. When HVDC cables are under load, a temperature gradient develops across the insulation, which results in a radial distribution of the insulation conductivity. A direct consequence is the accumulation of space charges within the insulation, which modifies the electric field across the insulation. The coupled problems due to electric field and temperature causes difficulties in identifying the electric field distribution in HVDC cables, which therefore a poses threat to the reliability in operation of DC power cables.

1.2 Objective

The main purpose of this master's thesis is to create a model that represents an insulation system of a submarine power cable. There are two challenges to overcome within this project; the first is to understand the physics of DC systems and the second is to establish such a model using numerical methods.

The model has to take into account both the electrical and thermal behavior in a HVDC cable. The specific objectives of the research are:

- To carry out theoretical descriptions of electric and thermal field calculations.
- To perform field calculations of the complex functions in the insulation.
- To analyze and to model the behavior under DC voltage where the conductivity varies with temperature gradient and affects the field.

1.3 Methods

The study in this work is carried out using a numerical calculation and simulation procedure. The axisymmetric geometry of the cable is used and a one-dimensional model is developed to study the electrical and thermal distribution across the insulation layer. In this thesis work, a MATLAB computer program is used, which provides accurate and fast numerical solutions to study the behavior of the cable.

In order to achieve the objectives, the following methods have been used:

1. A literature review and study of previous work.
2. Formulation of a theoretical description and coupled field calculation
3. Development of a model that can accurately describe the thermal and electrical couplings in the insulation.

1.4 Previous studies

Nonlinearity of dielectric materials and couplings between thermal and electrical phenomena in XLPE insulation layers have been studied by many researchers. A great deal of research on XLPE conductivity function [3] [4] by Steven Boggs, Institute of Material science, University of Connecticut, USA, has particularly paved the way for the work of this thesis. Further inspiration on numerical calculations has been found on the PhD thesis of Jinbo Kuang [5].

1.5 Outline of the thesis

Apart from this introduction, the report is structured into 6 chapters. A brief description of submarine power cable is given in Chapter 2 to provide a reader with basic information on physics of HVDC systems.

After this, governing mathematical equations that describe the insulation layer are derived and presented in Chapter 3. The most important numerical calculations can be found in Appendix A. Chapter 4 presents the model implementation and discusses the model geometry, material parameters and the way they are implemented in MATLAB. Chapter 5 presents the simulation results and explanations. Finally, Chapter 6 presents the conclusions and possible future work.

Chapter 2

Submarine High Voltage Direct Current Cables

"Direct Current is an abstraction which exists only at infinite time"- Prof. A. Pedersen. In the real world, all systems exist in a state somewhere between capacitive graded and resistively graded [3].

2.1 Background

Submarine power cables are the most significant elements in a HVDC power transmission between different zones. The reasons for the increased interest in using such systems in general and cable links in particular are [6] [7]:

- HVDC systems have lower transmission losses compared with HVAC. This is because they typically comprise only active power flow and this causes ~20% lower losses than HVAC system, which comprises both active and reactive power. Furthermore, the absence of skin and proximity effects in conductors makes HVDC cables especially attractive.
- When two neighboring AC systems operate at two different frequencies, for instance at 50 Hz and 60 Hz, HVDC is the only practical way for interconnection. This is because DC power is independent of the frequency and phase angle of the power systems and is free of reactive power. Therefore, power transmission with HVDC interconnection between two independent AC systems will not suffer from power swings.
- For the same power ratings, HVDC cables are more economical than HVAC cables due to less conductor and insulation material required.
- Since an HVDC cable draws negligible capacitive charging current, power can be transmitted through any length of it. The only limiting factors here are the cost and resistive losses.
- An HVDC transmission system is environmentally friendly because it improves power transmission allowing for interconnecting the existing power plants rather than building new power ones. This saves land compensation for new projects. In addition to this the absence of alternative electromagnetic fields in HVDC cables provides less health concerns.

2.2 HVDC Cable Insulation Technology

According to the type of insulation, HVDC cables can be categorized into two families: Cables with laminated insulation and with extruded insulation. There are different types of cables with laminated insulation, of which the mass impregnated (MI) cable is the most commonly used today. Crosslinked polyethylene (XLPE) is the most commonly used insulation material for extruded HVDC cables.

2.2.1 HVDC cables with laminated insulation

Among HVDC cables with laminated insulation, several technologies can be mentioned.

Mass impregnated (MI) paper: this insulation technology has been used for more than 100 years. The main advantages of MI cables are their long life time and long possible production length. The main drawback is that they are not suited for submarine installation due to high weight per length [8].

Mass impregnated paper polypropylene laminate (MI-PPL): this is a new installation technology which utilizes paper polypropylene laminate (PPL) material in order to improve the electrical and thermal performance of the mass impregnated cables [8].

Gas filled pre-impregnated paper insulation cables: this types of cable is no longer used today because it requires gas pressurization at the extremities and may experience uncontrolled water propagation in case of cable severance [8].

Self-contained fluid filled (SCFF) paper insulated cables: this type of cable can operate at both AC and DC voltages, with no change in cable design and manufacturing technology. However, due to the need for adequate oil feeding systems, there is a technical limitation in using these cables for long distances [8].

2.2.2 HVDC cables with extruded insulation

XLPE as insulation for HVDC cables offers significant advantage over the traditional laminated materials. The properties that make XLPE suitable for HVDC insulation are [8]:

- Low material and processing cost.
- Cable joints of extruded cables are much simpler and require less installation skill.
- The absence of oil leaks results in lower environmental hazards.
- Excellent moisture resistance and lighter cable.

On the other hand, HVDC cables with extruded insulation have been only recently employed while HVDC mass-impregnated cables have been proven to be reliable over many years [8].

Table 2.1 summarizes characteristics of MI and XLPE cables according to the existing installation and execution projects.

Table 2.1 Maximum data for HVDC cables [8]

	MI	XLPE
Maximum nominal operating voltage	600 kV MI-PPL (awarded) 500 kV MI (installed)	320 kV (awarded) 200 kV (installed)
Maximum continuous conductor temperature	70-80 °C (MI-PPL) 55-60 °C (MI)	70 °C
Conductor material	Copper/ Aluminum	Copper/ Aluminum
Maximum power (cable pair)	2200 MW (awarded) 1600 MW (installed)	900 MW (awarded) 400 MW (installed)
Maximum water depth	Approx 1600 m	Approx 400 m

2.3 Geometry of HVDC Cable

The design and configuration of HVDC submarine power cable is complex. For successful development of a HVDC submarine cables, several parameters must be carefully coordinated with the cable performance. Major characteristics such as ampacity, DC breakdown strength and cost should be analysed. The thickness of the insulation is a primary design parameter which influences all the above mentioned parameters [9]. A typical arrangement of submarine DC power cable is shown in the Figure 2.1 [10].

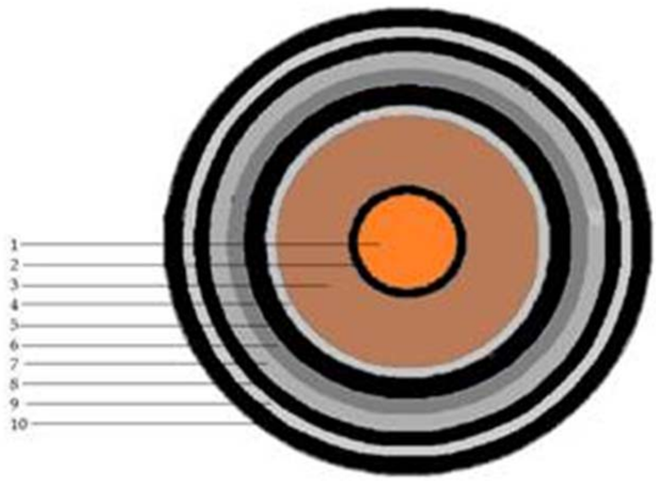

Fig 2.1: Typical construction of a submarine DC cable

The following components can be recognized:

1. Conductor: copper and aluminum are widely used for the conductor.
2. Conductor shielding: a semi-conducting layer which maintains a uniform electric field and minimizes electrostatic stresses.
3. Insulation: insulation material separates the current carrying conductor from the ground potential.
4. Insulation shielding: it is a semi- conductive layer which maintains a uniform electric field and minimizes electrostatic stresses.
5. Lead sheath: is used as a path for fault current during external cable damage and water barrier.
6. Plastic jacket
7. Tape armor bedding: it is used to provide a bedding for the armor wires.
8. Optical fiber: it is inserted for cable monitoring and communication purpose.
9. Wire armor: it is used with the lead sheath as a buried cable where moisture is a concern.
10. Serving: it is the final propylene sheath used as outer protective layer against corrosion and mechanical damage.

2.4 Difference between AC and DC Electric Field

"As the late Prof. A. Pedersen of the Danish Technical University liked to point out, DC is an abstraction which exists only at infinite time. In the real world, all systems exist in a state somewhere between capacitively graded and resistively graded." Cables designed for an AC system are designed to be only graded capacitively, since they are seldom subjected to a DC system. However cable for DC system are designed to be both capacitively and resistively graded [3].

2.4.1 Meaning of AC and DC grading

The difference of AC and DC grading can be realized by looking at the equations for the current density in the insulation. The total current density is the sum of the conduction current density J_c and displacement current density J_d [3].

$$J = J_c + J_d = \sigma E + \varepsilon_0 \varepsilon_r \frac{\partial E}{\partial t} \tag{2.1}$$

Here, E is the electric field strength, σ is the material conductivity, ε_0 is permitivity of free space, ε_r is the dielectric constant and t stands for time. In frequency domain, the displacement current due to sinusodial voltage excitation is $J_d = j\omega\varepsilon_0\varepsilon_r$, where ω is the angular frequency and j stands for the imaginary unit. In any way, the resistive current is proportional to the DC conductivity while the capacitive current is proportional to "ac conductivity" $\varepsilon_0\varepsilon_r\omega$. The nature of the field grading is determined by the dominating component, i.e if $\varepsilon_0\varepsilon_r\omega$ is greater than σ the system is capacitively graded and vice versa [3].

2.4.2 Electric Field in AC Cables

Calculation of electric field in AC cables is much easier compared to DC cables. In AC cables the electric field distribution depends on the permittivity of the insulation which is normally independent of the external parameters like temperature and the applied voltage. The field distribution in the insulation is capacitive. Therefore, it can be calculated with the Laplace equation in the absence of space charge [11].

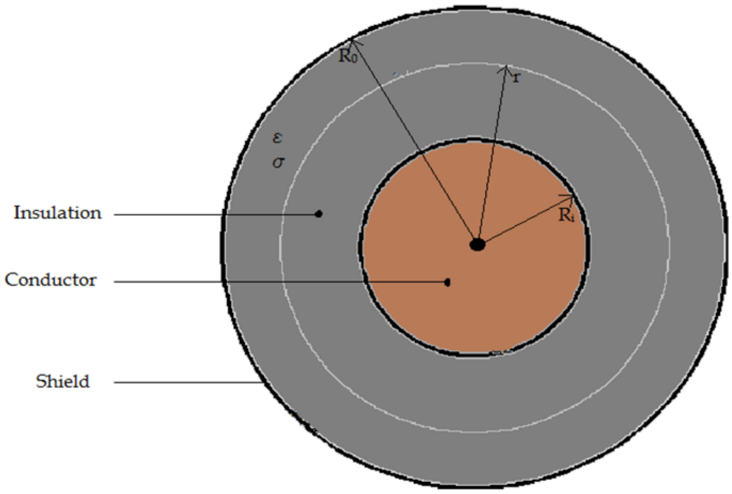

Fig 2.2: Simplified illustration of a cable

For a 1D axisymmetric domain (i.e a strait line connecting the centre of the cable and its external surface, Figure 2.2) Laplacian equation is expressed as:

$$\nabla^2 U = \frac{1}{r}\frac{\partial}{\partial r}\left(r\frac{\partial U}{\partial r}\right) \tag{2.2}$$

Here U is the electric potential and r is the radial co-ordinate. After integrating and setting a proper boundary condition, the geometrical electric field can be written as:

$$E(r) = \frac{U}{r\ln\left(\frac{R_0}{R_i}\right)} \tag{2.3}$$

Here, R_i and R_0 are the inner and outer radiuses of the insulation in m. Note that $R_i \leq r \leq R_o$ in Eq (2.3).

2.4.3 Electric Field in DC Cables

The calculation of electric field in cables under DC voltage is more complex. This is because the field distribution is controlled by material conductivity, which in case of XLPE is dependent on both the electric field and the temperature.

Different empirical formulas for conductivity of XLPE have been published, Thus in, [12], it is represented as a complex function of the two variables.

$$\sigma\,(\mathrm{E},\mathrm{T}) = \mathrm{A}\exp\left(\frac{-\phi \mathrm{q}}{\mathrm{k_B T}}\right)\frac{\sinh(\mathrm{B}\,|\mathrm{E}|)}{|\mathrm{E}|} \tag{2.4}$$

where A and B are constants, ϕ is thermal activation energy in *eV*, q is the charge of electron in *C*, T is temperature in *K*, E is the electric field in *V/m* and k_B is the Boltzmann constant.

According to [11], $\sigma\,(\mathrm{E},\mathrm{T})$ can be expressed as:

$$\sigma\,(\mathrm{E},\mathrm{T}) = \sigma_0 \exp(\alpha(\mathrm{T}-273)+\gamma|\mathrm{E}|) \tag{2.5}$$

where σ_0 is the conductivity at 0 °C and 0 *kV/mm*, α and γ are the temperature and electric field dependent coefficients respectively.

Even though Eq. (2.4) and Eq. (2.5) are different, they describe two important properties [12]:

1. σ(r) of the insulation increases with increasing electric field at a specific radius r.
2. σ(r) of the insulation increases with increasing temperature at a specific radius r

Since the thermal conditions within a cable change with time, this leads to dynamic variations of the electric field. Thus when a DC voltage is initially applied to a DC cable, high electric field stress occurs at the conductor screen as shown by solid curve in Figure 2.3. This is exactly the same as in case of AC cable. When the cable is fully loaded, a temperature gradient is developed due to the current flow and ohmic loss in the conductor and the previous situation starts to change. Increasing temperature leads to increasing conductivity at the conductor screen and decreasing conductivity at the insulating screen. This results in a high electric field stress at the insulation screen as shown by the dot curve in Figure 2.3 [13].

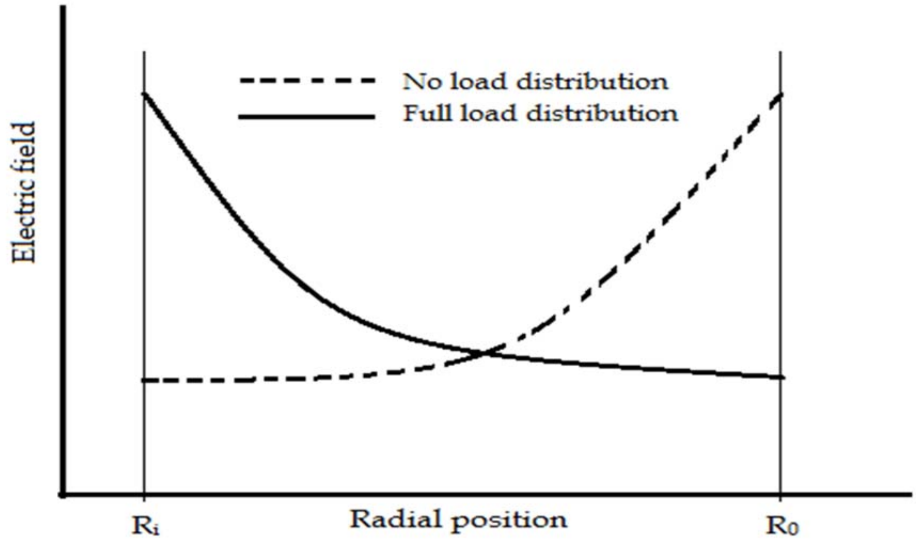

Fig 2.3: Electric field stress under load and no load condition in DC cable

Another important fact is that after voltage application, the field distribution is capacitive and it changes with time to a resistive type. In general, the behavior of the electric field distribution depends on the time variation of the applied stress and it linked to space charge build up in the insulation. An example is shown in Figure 2.4 (borrowed from [11] [14]) which indicates different stages in space charge dynamics in response to a time varying voltage.

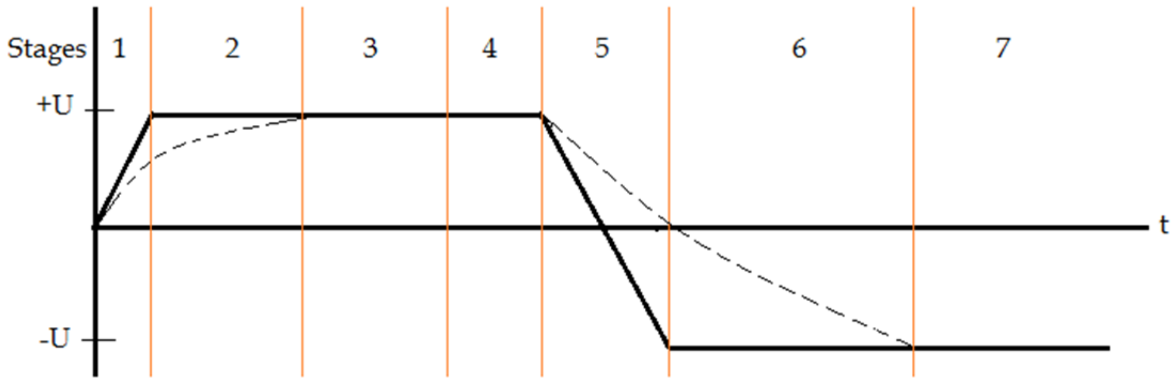

Fig 2.4: Different stages representing when a DC voltage is switched on/off. The dotted lines represent the development of space charges in the insulation.

<u>In the figure,</u>

stage 1: is the initial stage at which the cable is free of space charge and there is no temperature drop across the insulation. The field is controlled by the permittivity and geometry of the cable and has a purely capacitive distribution. The electric field can be calculated using Eq. (2.3).

Stage 2: In this stage the applied voltage attains its final voltage level. The field is time dependent. This stage is an intermediate stage between capacitive and resistive field distribution. The field and space charge can be calculated with Eqs. (2.10-2.12) and (2.15) discussed below.

Stage 3: The field in this stage is resistive and it is time independent. The load current is present resulting in a temperature gradient in the insulation. If such gradient in the insulation occurs, the effect of space charge exists which can be derived using Maxwell equation in Eq. (2.16). These space charges induce their own electric field causing field inversion as shown in Fig. (2.3).

Stage 4: The load current is turned off, the temperature drops and the cable cools down. For this reason, the field distribution changes to the initial case where highest field is found near the conductor. The theory described in stage 2 also holds in this stage. This stage is an intermediate and time dependent stage.

Stage 5: Two cases can be considered in this stage. First case without polarity reversal, following the turning off of the load current the voltage is decreased to zero. Due to the presence of space charge, the field gradually reduces to zero. The electric field is purely charge induced field. Hence, the field immediately after the voltage is switched off is calculated by:-

$$E(t = 0^{+}) = E(t = 0^{-}) - E_{AC} \tag{2.6}$$

Here $\mathrm{E}(\mathrm{t} = 0^{+})$ is the field just after the voltage is switched off, $\mathrm{E}(\mathrm{t} = 0^{-})$ is the field just before the voltage is switched off and $\mathrm{E_{AC}}$ is the capacitive field distribution as calculated in Eq. (2. 3).

The second case is considering polarity reversal of a loaded cable under a temperature gradient. Immediately after the polarity reversal of an external voltage source the space charge causes a high field stress to occur at the conductor. The field after polarity reversal is calculated similarly with Eq. (2. 6). However, $\mathrm{E_{AC}}$ in this case is twice the capacitive field distribution as the voltage changes from $+\mathrm{U}$ to $-\mathrm{U}$.

$$\mathrm{E_{AC}} = \frac{2\mathrm{U}}{\mathrm{r}\ln\left(\frac{\mathrm{R_o}}{\mathrm{R_i}}\right)} \tag{2.7}$$

Stage 6: This stage is an intermediate time dependent. The field gradually changes from the field calculated under stage 5 to stage 7. The field calculation in this stage is the same as in stage 2.

Stage 7: Finally the field at this stage becomes stable. The field is exactly the same but opposite in polarity to stage 3: $\mathrm{E_{stage\_7}} = -\mathrm{E_{stage\_3}}$

2.5 Electric Field with Field Dependent Conductivity

The electric field distribution across the insulation material is calculated assuming that the insulation consist of a weakly conducting material. The calculations require using Gauss law, current continuity equation, Ohm's law and gradient of the potential [2].

Gauss law:

$$\nabla \cdot \mathrm{E} = \frac{\rho}{\varepsilon_o \varepsilon_r} \tag{2.8}$$

Current continuity equation in differential form:

$$\nabla \cdot \mathrm{J} + \frac{\partial \rho}{\partial t} = 0 \tag{2.9}$$

Ohm's law:

$$\mathrm{J} = \sigma \mathrm{E} \tag{2.10}$$

Gradient of potential:

$$\mathrm{E} = -\nabla \mathrm{V} \tag{2.11}$$

In the formulas, E is the electric field strength in *V/m*, ρ is the space charge in *C/m³*, σ is the field dependent conductivity in *S/m*, J is the current density in *A/m²*, ε_o is permitivity of free space and ε_r is relative permitivity.

Combining the above four equations yields:

$$\frac{\partial}{\partial t}[\nabla \cdot (\varepsilon_0 \varepsilon_r \nabla \mathrm{V})] + \nabla \cdot (\sigma \nabla \mathrm{V}) = 0 \tag{2.12}$$

Assuming 1D cylindrical coordinate, Eq. (2.12) becomes:

$$\frac{\partial}{\partial t}\left[\frac{\partial}{\partial \mathrm{r}}(\mathrm{r}\varepsilon_0 \varepsilon_r \frac{\partial \mathrm{V}}{\partial \mathrm{r}})\right] + \frac{1}{\mathrm{r}}\frac{\partial}{\partial \mathrm{r}}\left(\mathrm{r}\sigma \frac{\partial \mathrm{V}}{\partial \mathrm{r}}\right) = 0 \tag{2.13}$$

Further the space charge can be calculated by substituting Eq. (2.10) into Eq. (2.11)

$$\rho = -\frac{\varepsilon_o \varepsilon_r}{\sigma}\frac{\partial \rho}{\partial t} + \mathrm{J} \cdot \nabla \left(\frac{\varepsilon_o \varepsilon_r}{\sigma}\right) \tag{2.14}$$

2.5.1 General Expression for DC electrical conductivity

The conductivity of XLPE is dependent of both electric field and thermal field. Hence to understand the conductivity of the polymeric material, both these factors have to be coupled. The coupling of electric field and thermal field occurs because the higher temperature of the insulation will result in increasing the electrical conductivity of the insulation. In turn, the higher conductivity will also cause a higher leakage current which will heat the insulation more. This process repeats untill an equilibrium is reached [15].

To understand the effect of electric field and temperature on conductivity of XLPE, a mathematical derivation has been developed according to charge hopping theory that gave a relation between the current density and electric field as a hyperbolic sine function [4].

$$J(E) = C\sinh(D|E|) \tag{2.15}$$

where C and D are constants, E is the electric field in *V/m.*

The dependency of the current density on temperature is given by;

$$J(T) = F\exp\left(\frac{-\phi . q}{k_B T}\right) \tag{2.16}$$

where F is a constant, ϕ is thermal activation energy in eV, q is elementary charge in *C*, k_B is the Boltzmann constant and T is the temperature in *K*.

Combining Eq.(2.15) with Eq.(2.16), one obtaines an expression for the the overall current density in the insulation:

$$J(E,T) = A\exp\left(\frac{-\phi q}{k_B T}\right)\sinh(B\,|E|) \tag{2.17}$$

From ohm's law,

$$\sigma(E,T) = \frac{J(E,T)}{|E|} \tag{2.18}$$

Substituting Eq. (2.17) in to Eq. (2.18) gives

$$\sigma\,(E,T) = A\exp\left(\frac{-\phi q}{K_B T}\right)\frac{\sinh(B\,|E|)}{|E|} \tag{2.19}$$

The expression in Eq. (2.19) couples the electric and thermal effects in the material.

2.6 Heat Transfer in HVDC Cables

Heat is defined as "a form of energy that can be transfered from one system to another as a result of temperature difference". Heat is transferred from high temperature medium to low temperature medium. There are three physical mechanisms of heat transfer: conduction, convection and radiation [16].

1. Conduction: Fourier law describes the heat transfer by conduction, specifying that the heat flux is proportional to the rate of temperature change over space. Eq. (2.20) shows Fourier law in cylinderical coordinate with only one radial direction [16].

$$Q = -kA\frac{dT}{dr} \tag{2.20}$$

Here, Q is the heat flux in *W*, k is the thermal conductivity of the material in *W/m ·K*, T is the temperature in *K* and r is the radial position in *m*. The negative sign in Eq. (2.20) indicates that heat always flow in the direction of decreasing temperature.

For underground transmission cables, heat conduction occurs everywhere except in the air space in the conduit. For overhead transmission cables, heat conduction occurs only inside the cable, the heat transfer ahead of the outer serving is due to convection and radiation [10].

2. Convection: Newton's law describes the heat transfer by convection. In simplest way, convection is defined as a transfer of heat from one place to another by the movement of a fluid (liquid or gases) [16]. The convective heat flux can be represented as:

$$Q = hA(T_s - T_\infty) \tag{2.21}$$

where Q is the heat flux in *W*, h is the convection heat transfer coefficient in *W/m² ·K*, A is the area in *m²*, T_s is the surface temperature in *K* and T_∞ is the ambient temperature in *K* from the surface.

For not buried submarine cables, convection take place from the cable surface to sea water. If a submarine cable installation is buried, the mode of the heat transfer is conduction [10].

3. Radiation: Radiation is the transfer of heat in the form of electromagnetic waves or photons. Unlike conduction and convection heat transfer by radiation doesn't require a medium and its intensity strongly dependent on temperature. Stefan-Boltzmann law describes the radiative heat transfer by radiation as being proportional to the difference of the temperatures at the power of four [16].

$$Q = \varepsilon\delta A\left({T_s}^4 - {T_\infty}^4\right) \tag{2.22}$$

Here Q is the emitted heat flux in *W*, ε is the emissivity of the surface of the object, that measures of how closely a surface approximates a black body and it is in the range $0 \le \varepsilon \le 1$, δ is the Stefen-Boltzmann constant 5.6703×10^{-8} *W/(m² ·K⁴)*, A is the surface area in *m²* ,T_s and T_∞ are surface and ambient temperature in *K* respectively.

2.7 Thermal field in DC cables

The temperature distribution across cable insulation is governed by the heat conduction equation [2].

$$\rho_m C_p \frac{\partial T}{\partial t} = \frac{1}{r}\frac{\partial}{\partial r}\left(rk\frac{\partial T}{\partial r}\right) + S_{heat} \tag{2.23}$$

where ρ_m is the mass density in *kg/m³*, C_p is the heat capacity in *J/kg ·K*, T temperature in *K*, k is temperature dependent thermal conductivity in *W/m ·K* and r is the radial position in m.

At high electric conductivity and field level, heat source that represents resistive losses in the insulation due to the current that passes through the insulation become significant. This resistive loss is given by:

$$S_{heat} = \frac{|J|^2}{\sigma} = \sigma|E|^2 \tag{2.24}$$

Here S_{heat} represents the resistive loss in the insulation in *W*, J is the current density in *A/m²* and σ is the conductivity in *S/m*. The second equality in Eq. (2.24) follows from Ohm's law in Eq. (2.10).

Chapter 3

Mathematical Modeling Equations

To understand the nonlinearity of Dielectric Materials, one should read in the language it is written and that language is Numerical Mathematics!

3.1 Introduction

The analysis of power cables is based on the solution of coupled field equations. The electrostatic field is defined by Maxwell's equation and the thermal field is defined by Fourier heat transfer equation. These equations are simple to formulate but difficult to solve due to the nonlinearity and time dependency.

Traditional methods of solving coupled field problems are based on the analytical approach with different simplification and approximations and the accuracy may be improved by using experimental data. The traditional methods are not efficient when high accuracy is required. Today, numerical methods are increasingly used for solving nonlinear coupled field problems. The development of different numerical schemes and computer powers has made it possible to solve more complicated and difficult tasks [5].

3.2 Finite Volume Method (FVM)

Classical finite difference methods approximates a solution of a differential equations using finite differences and it breaks down near discontinuities in the solution, where the equation does not hold. In this thesis, a finite volume method is utilized, which is based on an integral form of differential equation instead of the actual differential equation. Finite volume method discretizes domains into finite control volumes and approximates the total integral of the flux over each control volume rather than point wise approximations at mesh points. These values are modified on each time step by using the flux through the edges of the grid cells [17].

Finite volume methods are derived on the basis of the integral form of the conservation law. To understand how conservation laws arise from physical principles, let's consider a flux $\Phi(x,t)$, which is a one-dimensional quantity that varies with space x and time t.

$$\frac{d}{dt}\int_{x_1}^{x_2}\Phi(x,t)dx = f(\Phi(x_1,t)) - f(\Phi(x_2,t)) \tag{3.1}$$

Eq. (3.1) is the basic integral form of a conservation law for any two points x_1 and x_2. It is a very attractive feature of the finite volume method that the discretized equation has a clear physical interpretation. The above equation states that the rate of change of the total flux is due to only fluxes through the endpoints and it constitutes a balance equation for Φ over the control volume as shown in Fig 3.1 [17].

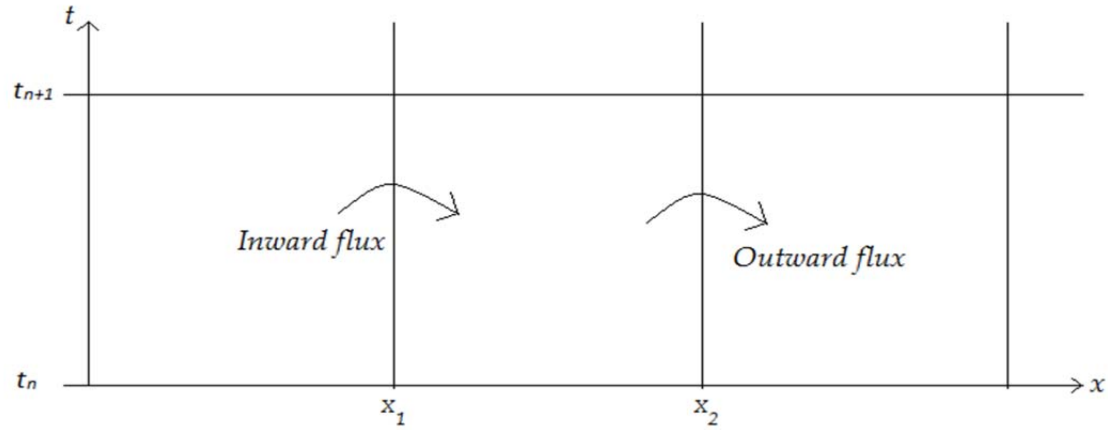

Fig3.1: Illustration of a finite volume method in x–t plane

3.3 Mathematical Derivation

As it was mentioned above, by combining Gauss's law, Ohms law and the current continuity equation, we get the electrical governing equation. In addition, Fourier law describes the heat transfer rate in the cable:

$$\begin{cases} \dfrac{\partial}{\partial t}[\nabla\cdot(\varepsilon_0\varepsilon_r\nabla V)] + \nabla\cdot(\sigma\nabla V) = 0 \\ \rho_m C_p \dfrac{\partial T}{\partial t} = \nabla\cdot(k\nabla T) + \sigma|E|^2 \end{cases} \tag{3.2}$$

To discretize Eq. (3.2), that is to convert a continuous differential equation to an algebraic discrete equations, it is integrated over a control volume in space and time.

$$\int_t^{t+\Delta t}\int_w^e \frac{\partial}{\partial t}\left[\frac{1}{r}\frac{\partial}{\partial r}(r\varepsilon_0\varepsilon_r\frac{\partial V}{\partial r})\right]drdt + \int_t^{t+\Delta t}\int_w^e \frac{1}{r}\frac{\partial}{\partial r}\left(r\sigma\frac{\partial V}{\partial r}\right)drdt = 0 \tag{3.3}$$

$$\int_t^{t+\Delta t}\int_w^e \rho_m C_p\frac{\partial T}{\partial t}drdt = \int_t^{t+\Delta t}\int_w^e \frac{1}{r}\frac{\partial}{\partial r}\left(rk\frac{\partial T}{\partial r}\right)drdt + \int_t^{t+\Delta t}\int_w^e S_{heat}\,drdt \tag{3.4}$$

(for a detailed numerical calculation see Appendex A).

3.3.1 Discretization in space

Unlike the finite difference, which discretizes solution at individual points, in the finite volume method one divides the spatial domain into cells of control volume. A "finite volume" refers to the small volume surrounding each node on a mesh and faces of a control volume are positioned midway between adjacent nodes [17].

Figure 3.2 shows a single control volume of width $\Delta r = \delta_{rwe}$. The nodal point is defined as P whereas E and W are the two neighbor nodes to the east and west respectively. The west and east side faces of the control volume are identified by w and e, respectively [18].

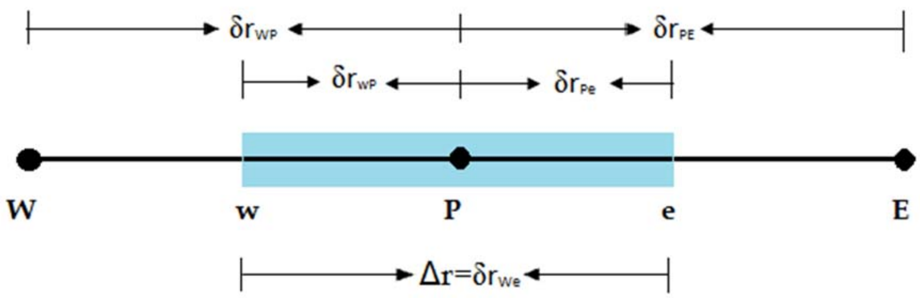

Fig 3.2: Finite volume grid

The gradients at the faces of the control volume are calculated using the values at the two negbour nodes using a central difference formula.

$$\left(\frac{\partial \Phi}{\partial r}\right)_w = \left(\frac{\Phi_P - \Phi_W}{\delta r_{WP}}\right) \tag{3.5}$$

$$\left(\frac{\partial \Phi}{\partial r}\right)_e = \left(\frac{\Phi_E - \Phi_P}{\delta r_{PE}}\right) \tag{3.6}$$

Here, Φ_P, Φ_E and Φ_W are fluxes (in the electrical equation the flux is the electric potential and in the thermal equation it is the temperature) at nodal points P, E and W, respectively; δr_{WP} is the radial distance between the west node and the point node. Similarly, δr_{PE} is the radial distance between the point node and the east node.

For a uniform grid, a linear interpolation can be used to evaluate the diffusion coefficients(i.e material characteristics in the electric and thermal equation).

$$\Gamma_w = \frac{\Gamma_W + \Gamma_P}{2} \tag{3.7}$$

$$\Gamma_e = \frac{\Gamma_P + \Gamma_E}{2} \tag{3.8}$$

Here, Γ_w and Γ_e are the diffusion coefficients at the west and east faces of the control volume; Γ_W, Γ_P and Γ_E are diffusion coefficients at nodal points P, E and W respectively. In the coupled Eq. (3.2), the diffusion coefficient for the electrical equation is the electrical conductivity and for the thermal equation it is the thermal conductivity.

3.3.2 Discretization in time (Time stepping)

In order to solve nonlinear problems in time domain, the coupled partial differential equation must be discretized using some time stepping algorithm which allow for solving the differential equation at each time step.

To evaluate the integrals of Eq. (3.3) and Eq. (3.4), an assumption is made about the variation of the flux with time. One may use a flux at time t or at time $\mathrm{t} + \Delta\mathrm{t}$ to calculate the time integrals, or alternatively the combination of the fluxes at times t and $\mathrm{t} + \Delta\mathrm{t}$. One can generalize this approach by means of a weighting parameter θ with values between 0 and 1 and to write the integral with respect to time as [18]:

$$\int_{t}^{t+\Delta t} \Phi_P \, \mathrm{dt} = \left[\theta \, \Phi_P{}^{t+\Delta t} + (1-\theta) \, \Phi_P{}^{t}\right]\Delta t \tag{3.9}$$

Here, $\Phi_P{}^{t+\Delta t}$ is the new flux at time $t + \Delta t$ and $\Phi_P{}^{t}$ is the old calculated flux at time t. Depending on the parameter value, different schemes can be obtained. Thus if $\theta = 0$, the flux at the old time level t is used. If $\theta = 1$ the flux at new time level $\mathrm{t} + \Delta\mathrm{t}$ is used; and finally if $\theta = 1/2$ the flux at t and $\mathrm{t} + \Delta\mathrm{t}$ are equally weighted. The obtained approximations and their properties are summarizedin Table 3.1. As seen, the Crank Nicolson scheme has the advantage of being very stable and provides more accuate results than the Forward and Backward Euler method. Therefore for the dynamic problems defined in this thesis, the Crank-Nicloson method is implemented.

Table 3.1 Time stepping schemes

θ	0	1/2	1
Name	Forward Euler(FE)	Crank Nicolson(CN)	Backward Euler(BE)
Result	$\Phi_P{}^{t}\Delta t$	$\frac{1}{2}\left(\Phi_P{}^{t+\Delta t} + \Phi_P{}^{t}\right)\Delta t$	$\Phi_P{}^{t+\Delta t}\Delta t$
Stability	Conditionally stable	Unconditionally stable	Unconditionally stable
Accuracy	First order	Second order	First order

3.4 Boundary Conditions

For the electrical problem, boundary conditions are needed for the electric potential . Therefore, the conductor screen is assumed to be at 150 kV voltage level while the potential is assumed to be zero at the insulation screen.

For the thermal problem, heat generation of a conductor is considered and the heat flux at the inner conductor is set to 52.5 W/m, which results in a steady state conductor temperature of 70 ℃. A convection-radiation boundary condition is encountered on the outer surface of the cable as it is exposed to the temperature of the surrounding environment. The thermal boundary condition can be derived using the Cauer type ladder network.

3.4.1 Cauer RC ladder network

The network represents various layers of the power cable by thermal resistances and thermal capacitances. The heat generated in the conductor travels thorough the thermal resistance and thermal capacitance and finally to the outer layer towards the ambient environment. The Cauer ladder network is modeled similarly to an analogous electrical circuit while electric potential are equivalent to temperatures and electric currents to heat fluxes [19].

The thermal resistance characterizes material's ability to impede heat flow [19]. Thus, the thermal resistance of the metalic conductor is small due to relatively high thermal conductivity and it is given as:

$$\mathrm{R}_1 = \frac{1}{4\pi \mathrm{k}} \tag{3.10}$$

All insulating layers in the cable impede heat flow away from the conductor. The expressions for the thermal resistances of layers can be found by solving the steady state Fourier heat equation that yields:

$$R = \frac{\ln\left(\frac{\mathrm{r_o}}{\mathrm{r_i}}\right)}{2\pi \mathrm{k}} \tag{3.11}$$

In the equations, R is thermal resistance in *mK/W*, k is the thermal conductivity in *W/mK*, $\mathrm{r_o}$ and $\mathrm{r_i}$ are the outer and inner raduis of the layer in *m*.

The thermal resistance at the external boundary accounts for convection and radiation. Since the convective heat flux is given by Eq. (2.21), the thermal resistance for convection is then:

$$R_{conv} = \frac{T_s - T_\infty}{q} = \frac{1}{hA} \tag{3.12}$$

Radiation exchange between the cable surface and its surroundings is introduced by Eq. (2.22) and the corresponding thermal resistance can be defined as:

$$R_{Rad} = \frac{T_s - T_\infty}{q} = \frac{T_s - T_\infty}{\varepsilon\delta A({T_s}^4 - {T_\infty}^4)} \tag{3.13}$$

A thermal capacitance of a material characterises it's ability to store heat and it is given by [19]:

$$C = \rho_m C_p \pi({r_o}^2 - {r_i}^2) \tag{3.14}$$

where ρ_m is the mass density in *Kg/m³* and C_p is the heat capacity in *J/KgK*.

The network used in present study is shown in Figure 3.2, where R1 upto R6 represent the thermal resistances of each layer shown in Figure 4.1, R7 is the thermal resistance due to convection-radiation boundary condition and C1 upto C6 represent thermal capacitance of each layer.

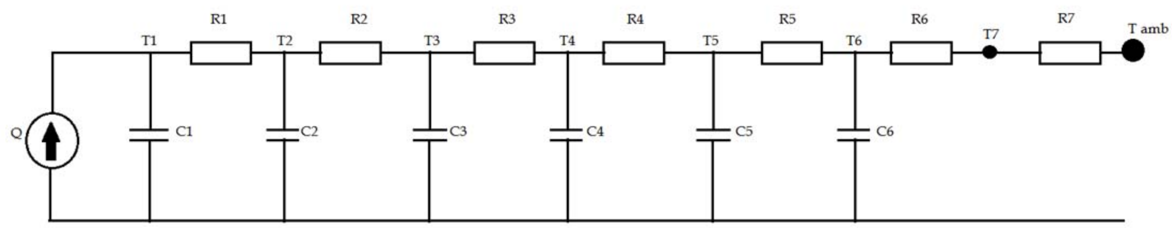

Fig 3.2: Cauer ladder network representing a cable

Chapter 4

Model Implementation

A model (from Latin modulus) is a representation of reality. The first task in modeling is to identify the system under study and approximate the real geometry to an ideal geometry and approximating material properties.

4.1 Introduction

A MATLAB program has been developed according to the finite volume method for solving coupled transient nonlinear field problems based on the numerical techniques pointed out on previous chapter.

4.2 Model Description and Definition

4.2.1 Cable Geometry

This thesis focuses on a 150kV XLPE HVDC cable. Its simplified structure is shown in Figure 4.1 and the dimensions are provided in table 4.1. The geometry has been implemented in cylindrical coordinates and the problem was reduced to 1D utilizing radial symmetry.

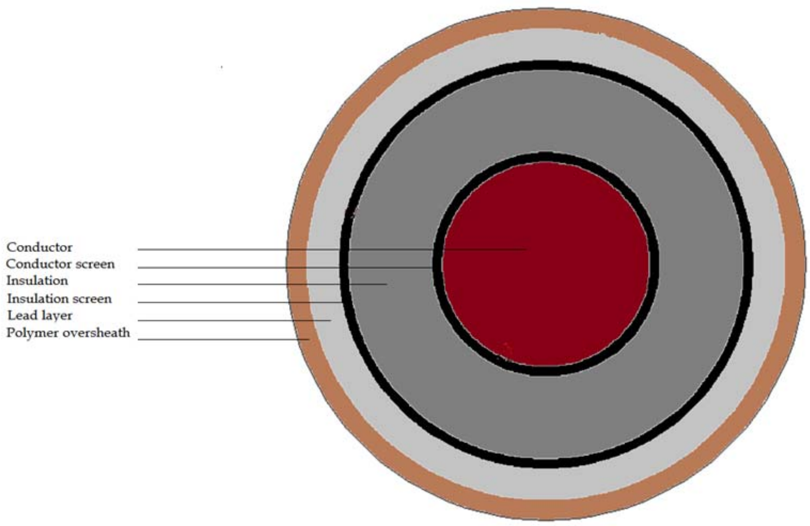

Fig 4.1: Cable Geometry

Table 4.1 Cable dimensions [20]

Material	Radius [*mm*]
Aluminum conductor	10
Conductor screen	11
Insulation layer	19
Insulation screen	20
Lead layer	23
Polymer oversheath	25

4.3 Material Parameters

The parameters of the materials of the cable are summarized in Table 4.2.

Table 4.2 Material data [20]

Material	$\rho[kg/m^3]$	$C_p[J/kgK]$	$k[W/mK]$
Aluminum conductor	2700	890	200
Conductor screen	1100	2050	0.47
Insulation layer	920	2250	0.329
Insulation screen	1100	2050	0.47
Lead layer	11340	125	35
Polymer oversheath	920	2250	0.329

Note that in general, the heat capacity of the materials is dependent on both pressure and temperature, but this dependency is not imporatnt in the present study. The permittivity of the insulation can be considered as constant ($\varepsilon_r = 2.3$) within the relevant range of temperatures and fields.

4.4 Numerical Solution of Nonlinear systems

To solve the problem, the insulation is split into a number of radial control volumes with thickness Δr. Each discretized control volume is characterized by the following quantities, which in general are functions of radius r and time t:

- Electric potential $V(r,t)$
- Temperature $T(r,t)$
- Electric field $E(r,t)$
- Conductivity $\sigma(T(r,t),E(r,t))$
- Current density $J(r,t)$
- Space charge $\rho(r,t)$

A computer code implementing the FVM approach for solving the transient axisymmetric coupled nonlinear field problem has been developed utilizing the techniques introduced in in section 3.2.1 and 3.2.2. Thus, finite volume discretization of Eq. (3.3) and Eq. (3.4) yields, the algebraic equations Eq. (4.1) and Eq. (4.2):

$$\mathrm{V_P} = \frac{\mathrm{a_{EV}V_E} + \mathrm{a_{WV}V_W} + \mathrm{a_{EV0}V_E}^{0} + \mathrm{a_{WV0}V_W}^{0} + \mathrm{a_{PV0}}\,\mathrm{V_P}^{0}}{\mathrm{a_{PV}}} \tag{4.1}$$

Here, V_E, V_W and V_P are the potentials at the new time level $t + \Delta t$; $V_E{}^0$, $V_W{}^0$ and $V_P{}^0$ are the potentials at the preceeding instant t. Similarly for the thermal problem

$$\mathrm{T_P} = \frac{\mathrm{a_{ET}T_E} + \mathrm{a_{WT}T_W} + \mathrm{a_{ET0}T_E}^{0} + \mathrm{a_{WT0}T_W}^{0} + \mathrm{a_{PT0}}\,\mathrm{T_P}^{0} + \mathrm{S_{heat}}}{\mathrm{a_{PT}}} \tag{4.2}$$

where, T_E, T_W and T_P are the temperature levels at the new time level $t + \Delta t$; $T_E{}^0$, $T_W{}^0$ and $T_P{}^0$ are the temperatures at the preceeding instant t.

By extending the above equations over the entire insulation, the problem is reduced to a matrix form.

The quantities mentioned above are calculated in each finite volume for each instant with a time interval Δt. Solution of the matrix problem is obtained using Gauss Sediel iteration method until the solution is converged and a predefined time has been reached.

The flow chart below shows the general flow of the FVM program.

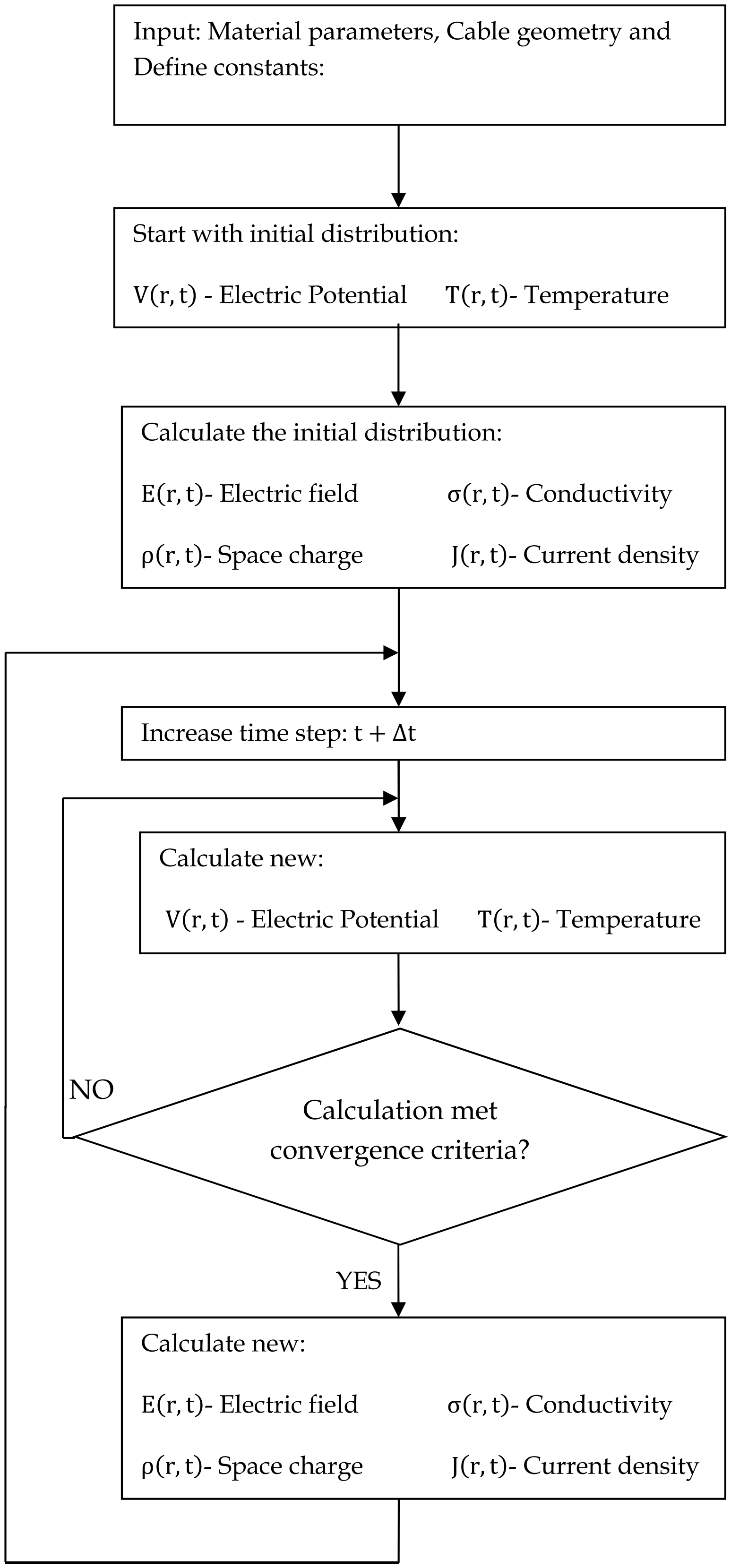

Fig. 4.2: Flow chart of field calculation

4.4.1 Convergence Criteria

The iterative algorithm used requires some stopping conditions. The convergence criteria in the present study were defined by considering the residuals for both electric (R_E) and thermal (R_T) differential equations.

$$\begin{cases} R_E = \sum_{All\ Nodes} \left|\mathrm{a_{ET}V_E + a_{wT}\,V_W + a_{EV0}V_E}^{\ 0} + \mathrm{a_{WV0}V_W}^{\ 0} + \mathrm{a_{PV0}\,V_P}^{\ 0} - \mathrm{a_{pT}V_P}\right| \\ R_T = \sum_{All\ Nodes} \left|\mathrm{a_{ET}T_E + a_{wT}\,T_W + a_{EV0}T_E}^{\ 0} + \mathrm{a_{WV0}T_W}^{\ 0} + \mathrm{a_{PV0}\,T_P}^{\ 0} - \mathrm{a_{pT}T_P}\right| \end{cases} \quad (4.3)$$

These were normalized to be able to judge whether the equation system has converged or not. The criterion for convergence was then [21]:

$$\frac{R_E}{F} \leq \varepsilon \text{ and } \frac{R_T}{F} \leq \varepsilon \quad (4.4)$$

where

$0.0001 \leq \varepsilon \leq 0.01$

Note that F in Eq. (4.4) represents the total flux of the dependent variable. In the case of the electrical equation it represents the total current, and in case of the thermal equation it represents the total heat transfer rate.

4.5 Thermal boundary conditions

As explained in section 3.4.1, the boundary conditions are time dependent and the outer thermal boundary condition accounts for radiation, which is represented by a nonlinear thermal resistance. To improve the accuracy of the Cauer RC ladder network, the thermal resistance of each layer is divided into two parts, and the capacitance is defined at the middle. This improves the accuracy of the approximation. The RC ladder thermal network was implementd in Simulink, as shown in the Figure 4.3 below.

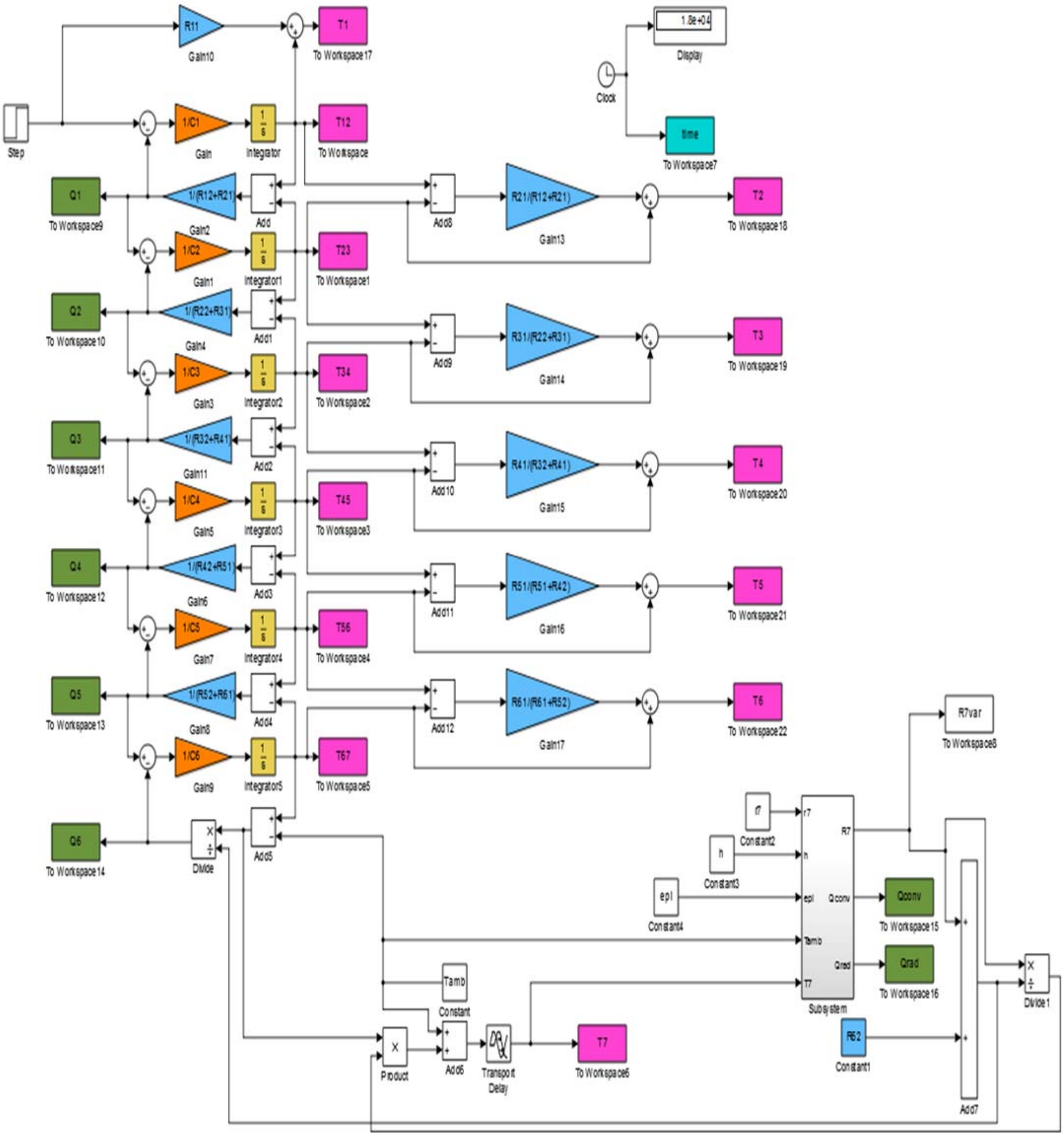

Fig. 4.3: Simulink Cauer type RC ladder network diagram

Chapter 5

Results and Discussion

5.1 Introduction

The simulation results are mainly discussed into two section, the steady state and transient studies.

5.2 Steady state study

In this study, the simulations are carried out under the assumption that the system is in a steady state and that the temperature on the surface of the conductor is constant. Temperature distributions in the insulation at different temperature gradient within the cable are shown in Figure 5.1. The temperature differences across the insulation has a significant influence on the electric field distribution as shown in Figure 5.2.

As it is seen, the electric field strength is higher at the inner conductor than at the outer boundary of the insulator when the temperature gradient is small. With larger temperature gradients in the insulation, the electric field profile reverses.

Figure. 5.3 shows the effect of temperature gradient on the conductivity distribution in the insulation. It is clear from the figure that the conductivity is a strong nonlinear function of the temperature.

Temperature gradient lead to presence of space charge across the insulation due to temperature and field dependency of the conductivity. The space charge density is calculated using Eq. (2.13), which in a steady state becomes:

$$\rho = J \cdot \nabla \left(\frac{\varepsilon_o \varepsilon_r}{\sigma} \right) \tag{5.1}$$

As follows from Eq.(5.1), conditions for space charge accumulation across the insulation are defined by the dielectric time constant:

$$\tau = \frac{\varepsilon_o \varepsilon_r}{\sigma} \tag{5.2}$$

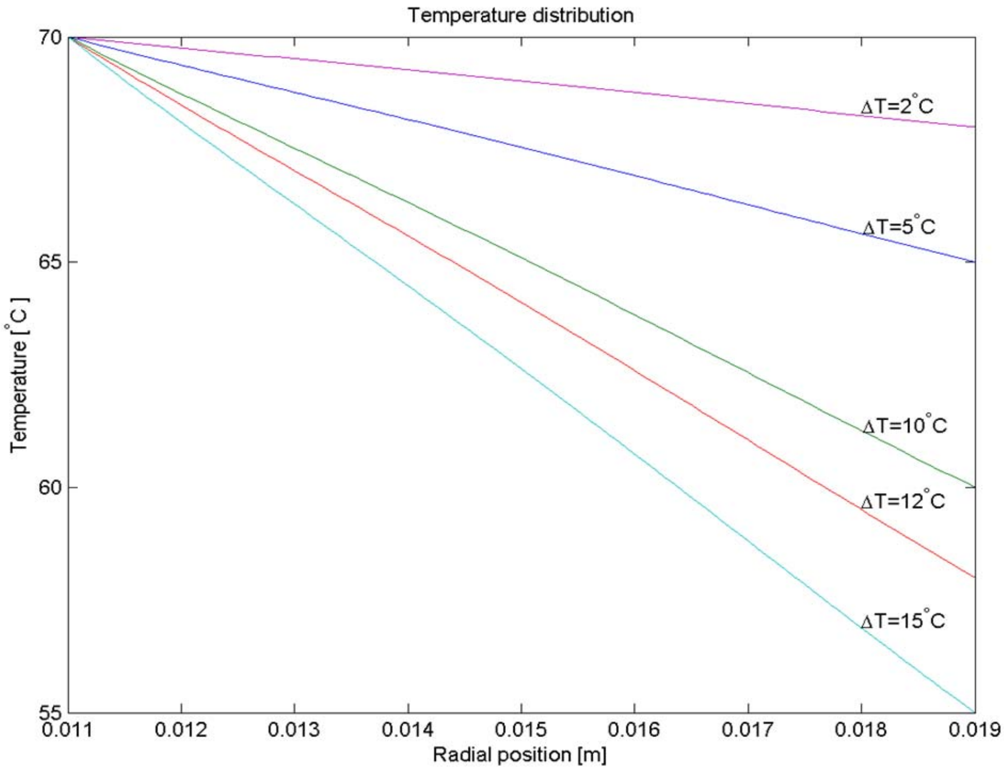

Fig.5.1: Temperature distribution across the insulation at different ΔT with $\phi = 0.56\mathrm{eV}$

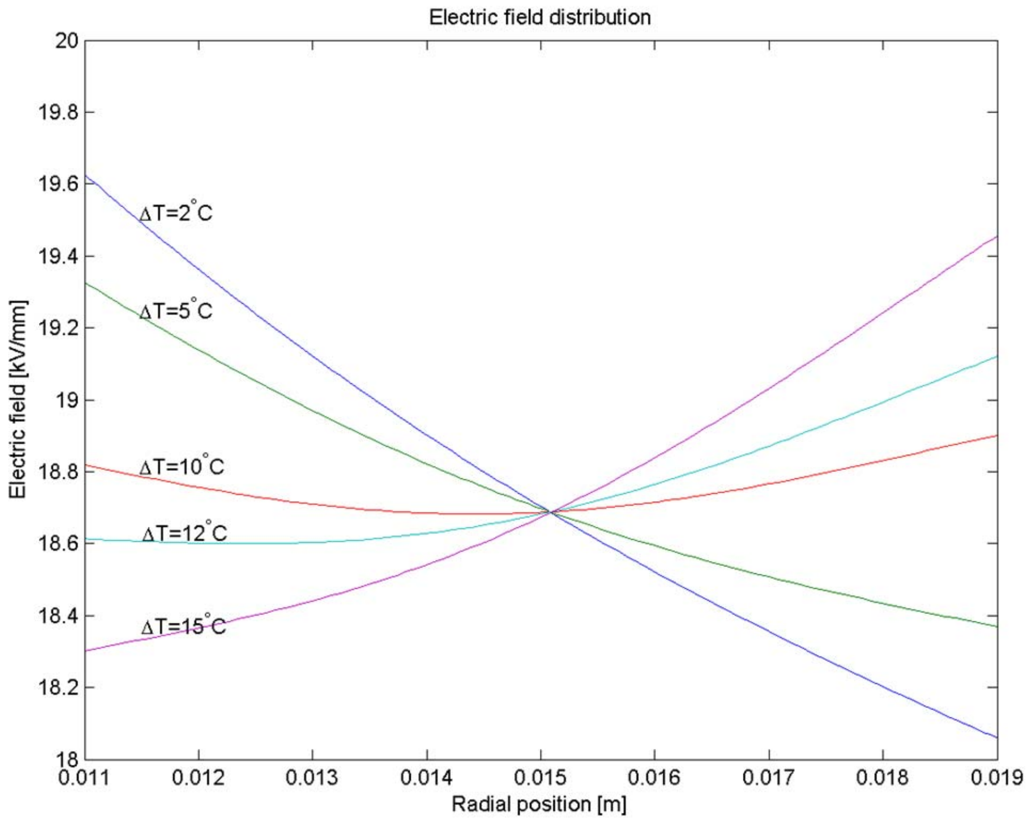

Fig.5.2: Electric field distribution across the insulation at different ΔT with $\phi = 0.56\mathrm{eV}$

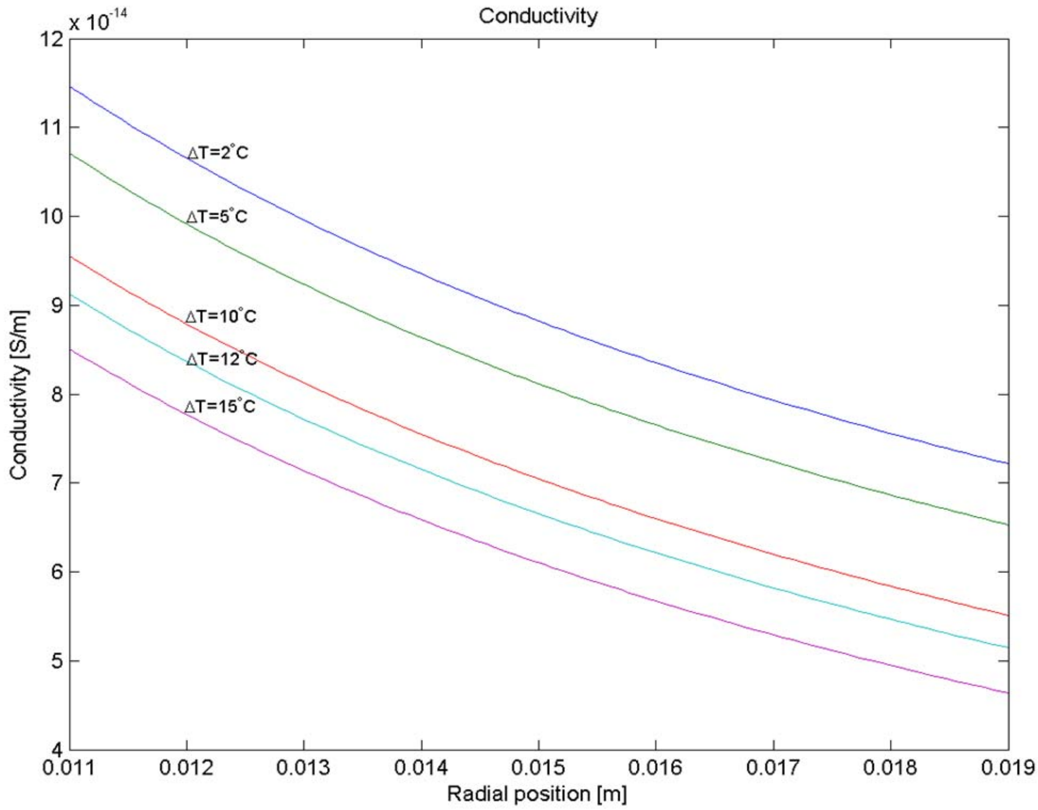

Fig.5.3: Conductivity across the insulation at different ΔT with $\phi = 0.56\mathrm{eV}$

If the conductivity of the material is constant, the ratio constant, ${\varepsilon_0 \varepsilon_r}/{\sigma}$ is also constant and its gradient is zero that results in zero space charge according to Eq. (5.1).

However, the situation changes when a temperature gradient occurs in the insulation due to the heating originating from the conductor. The conductivity varies with the electric field and temperature, a temperature gradient generates a conductivity gradient and thus the permittivity to conductivity ratio ${\varepsilon_0 \varepsilon_r}/{\sigma}$ will vary. Therefore, space charge is accumulated across the insulator and the amount of space charge increases with the temperature drop across the insulator as shown in Figure 5.4.

In addition to the dependency on electric field strength and temperature, the conductivity of XLPE is also thermally activated. Thermal activation energy is defined as the least amount of energy needed for chemical reactions enhancing rates of conduction processes to take place. The conductivity of most dielectric materials is thermally activated with an activation energy in the range of 0.5eV-1.5eV. As seen from Eq. (2.19) decreasing the activation energy weakens the temperature dependency of the conductivity across the insulation and as a result, the field becomes more uniform under DC stress, as shown in Fig 5.5. Therefore, a low activation energy is desirable for insulating materials, however, they should still provide low leakage current through the insulation.

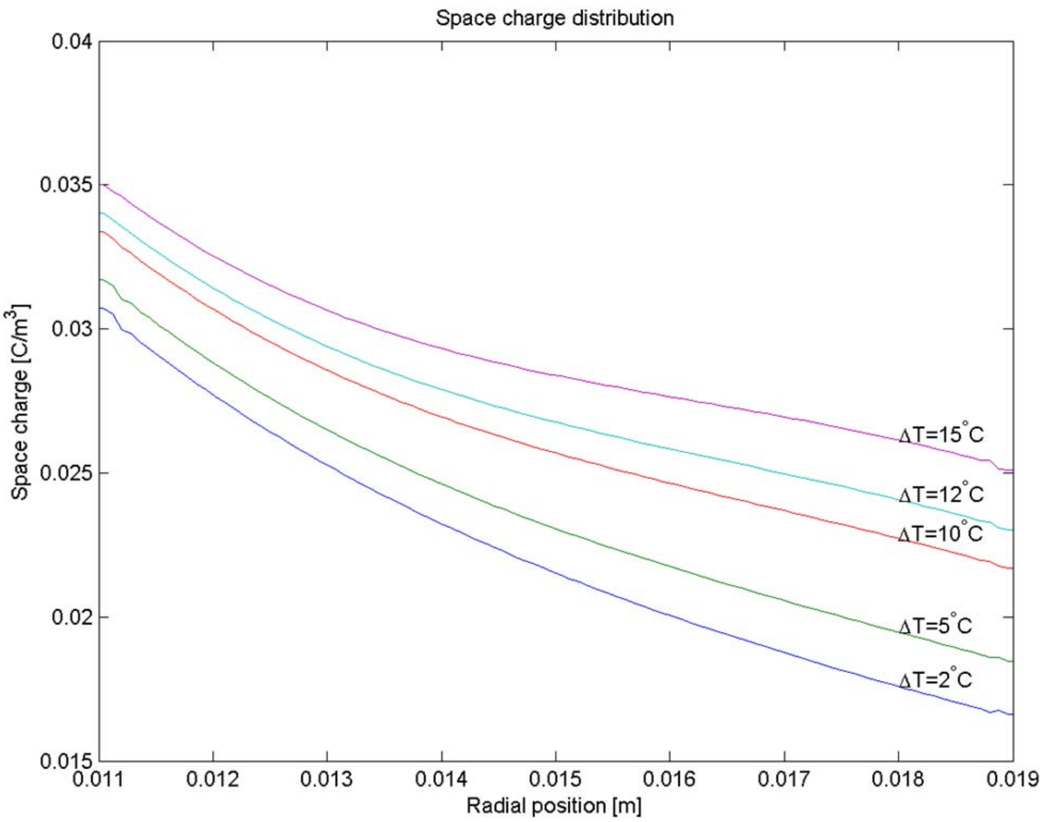

Fig.5.4: Space Charge distribution across the insulation at different ΔT with $\phi = 0.56\text{eV}$

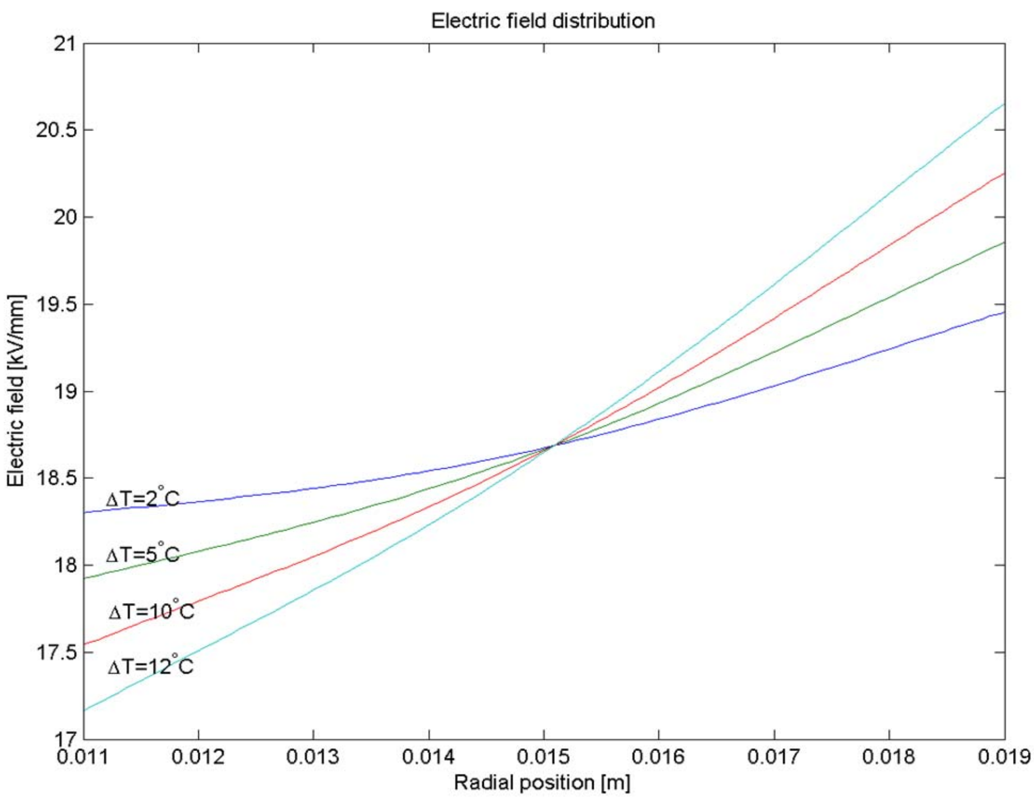

Fig.5.5: Electric field distribution across the insulation at different ϕ with ΔT=15℃

5.3 Transient study

Solution of the coupled nonlinear equations Eq.(3.2) requires, a set of consistent boundary and initial conditions. In the present study, an exponentially decaying electric potential the analytical solution of Laplace equation Eq. (2.2) and a flat ambient temperature profile across the insulation layer are taken as intial distributions, see plots in the left column in Fugure 5.6.

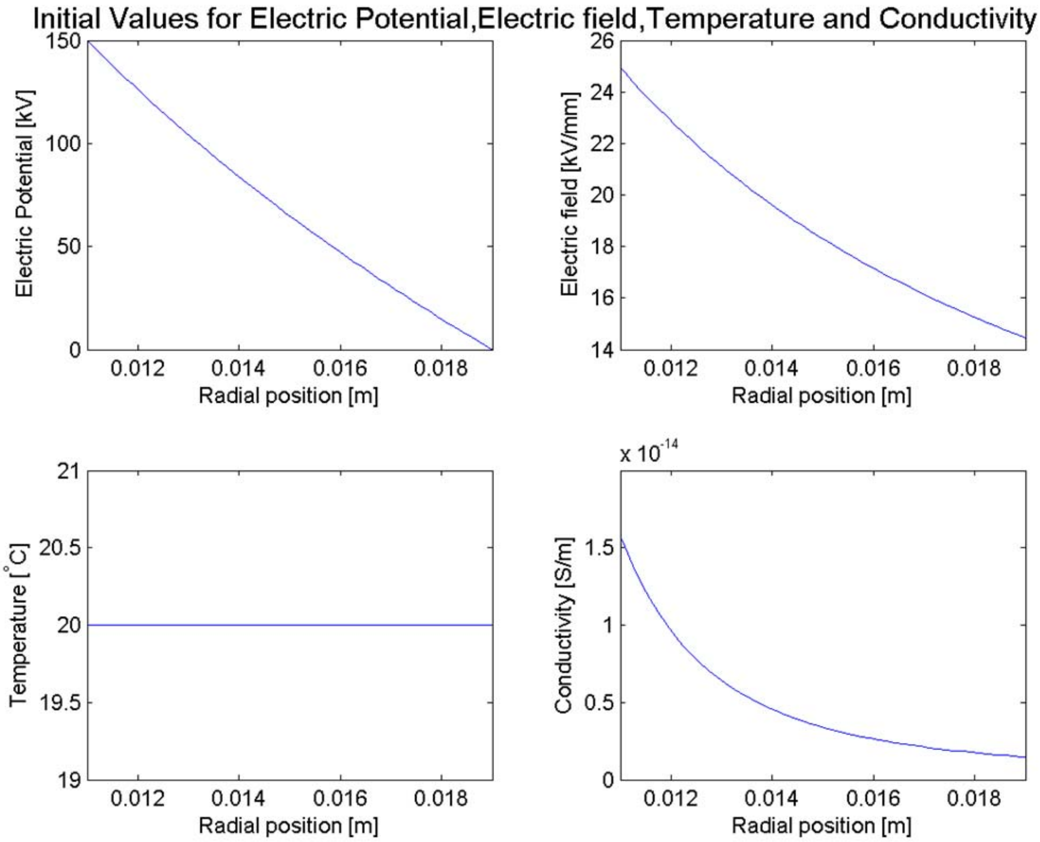

Fig. 5.6: Initial values for electric potential, electric field, temperature and conductivity distribution across the insulation

5.3.1 Time dependent boundary condition

The thermal boundary condition on the insulation layer is time dependent. To accommodate the time dependency, the conductor heating on the conductor screen and convection-radiation boundary condition on the outer surface of the cable are encountered. Based on the modelling with the RC ladder circuit, T3 and T4 represents the temperatures on the inner and outer part of the insulation layer respectivly and their time variations are shown in Figure 5.7. An important point to notice concerning the equivalent thermal circuit model in Figure 3.2 is that the nonlinear temperature dependence of the radiation heat transfer on the outer surface of the cable was taken into account as well as conduction and convection heat

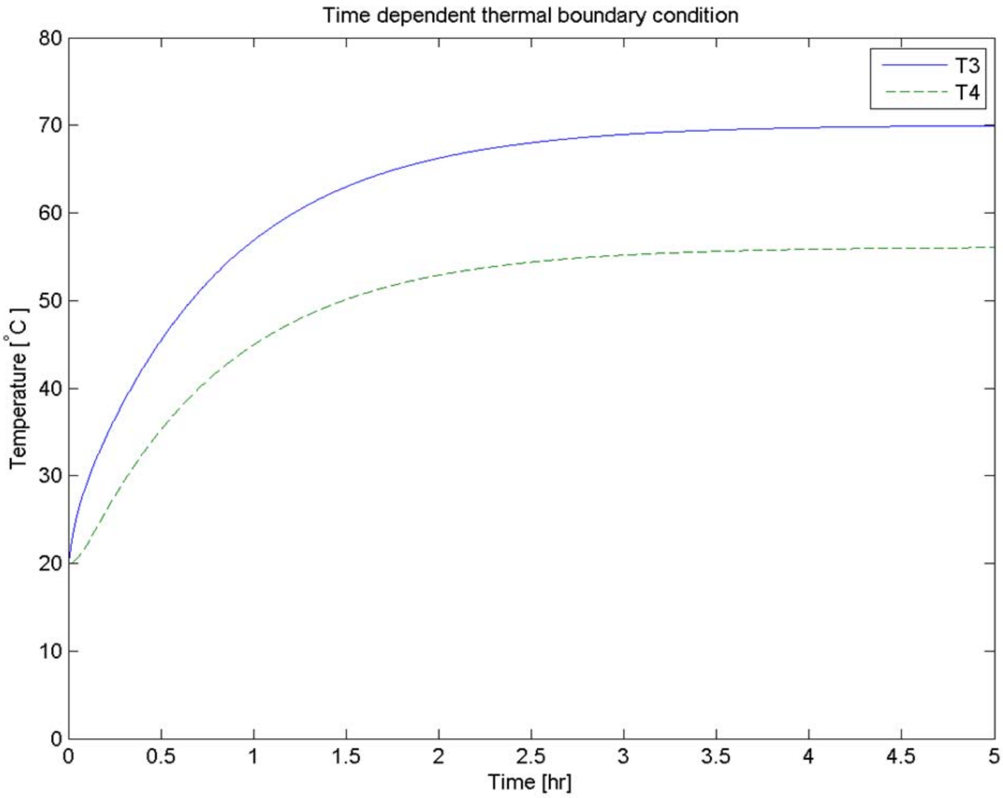

Fig.5.7: Time dependent boundary condition for temperature

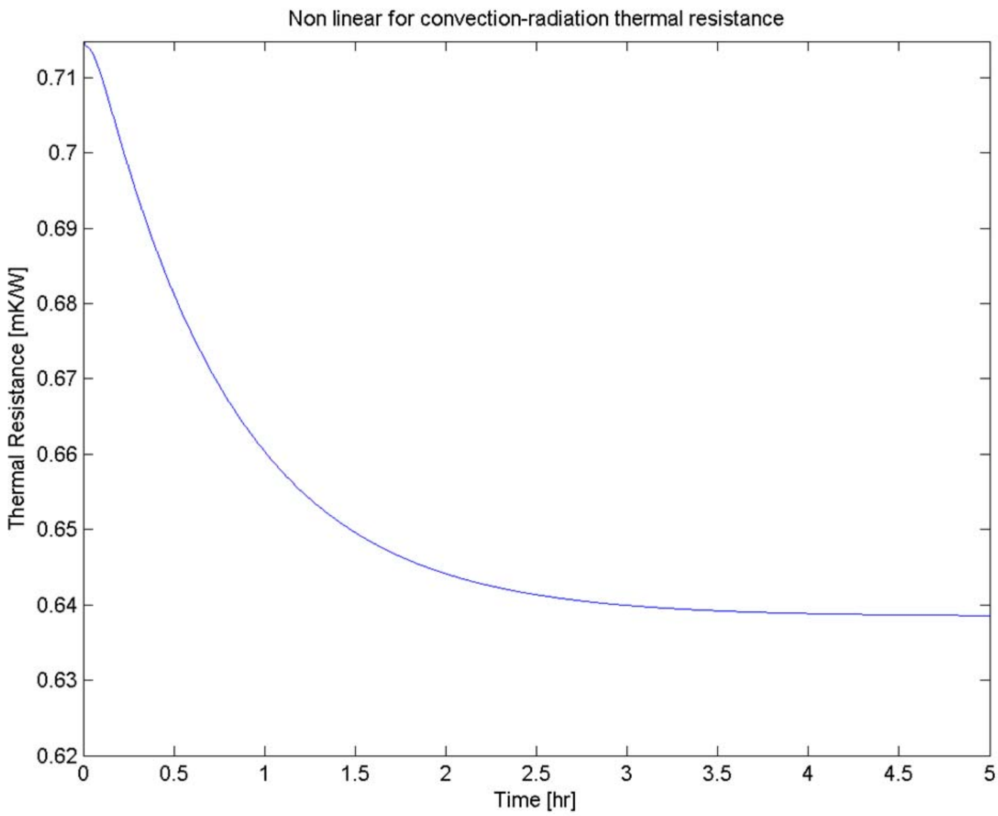

Fig.5.8: Non-linear thermal resistance

transfer. The latter are linear with assuming that h and k are temperature independent. Hence, the nonlinear thermal reistance R7 varies at the beginning of the simulation and it attined a steady state value with time as shown in Figure 5.8.

5.3.2 Time dependency and field inversion

As was mentioned in the steady state study, the temperature difference across the insulation layer has a considerable effect on the electric field distribution of the insulation layer. The solution of the dynamic problem, Figure 5.9, shows how the temperature gradient develops with increase of the temperature over time. The corresponding distribution of the electric field at different instants are presented in Figure 5.10.

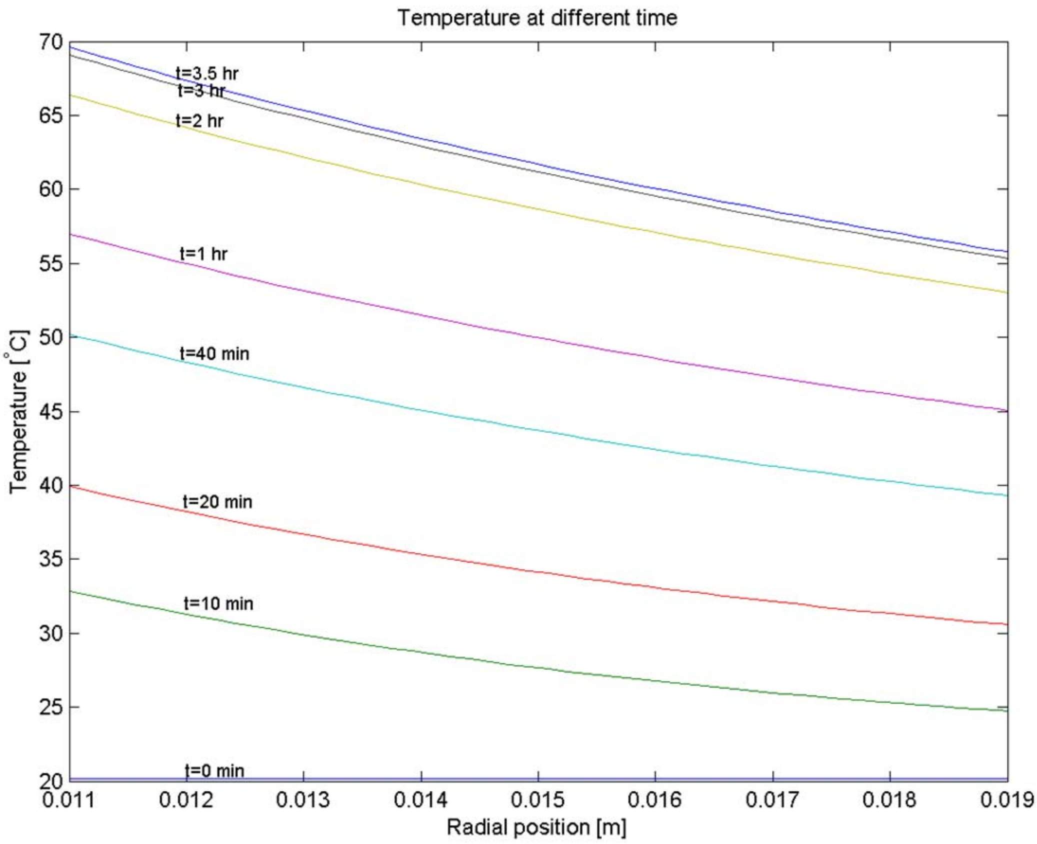

Fig.5.9: Temperature distribution across the insulation at different time

As it is seen , at the beginning whena DC voltage is applied, the electric field profile is capacitivle type. With time, the temperature gradient builds up which results in a decrease of the electric field at the inner part of the insulaion and its increase in the outer part of the insulation layer. This is due to the fact that the inner part of the insulation is warmer than the outer region and the resulting electric conductivity of the inner part of the insulation is higher than that of the outer part. A pure resistive electric field can be achieved only at infinite time.

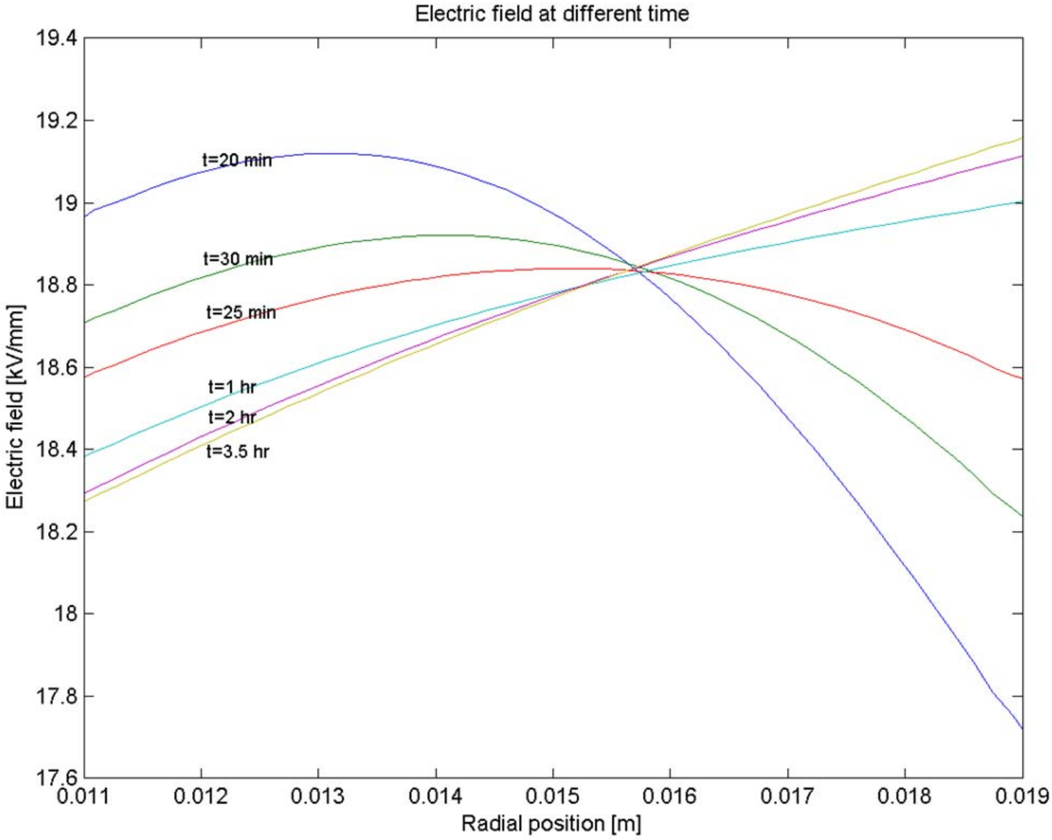

Fig.5.10: Electric field distribution across the insulation at different time

5.3.3 Build up of space charge across insulation layer

The nonlinear behaviour of the electric conductivity leads to space charge build in the insulation. The dynamics of the process is shown in Figure 5.11. One can observe that the amount of the charge is higher in warmer regions of the insulation due to higher conductivities. For the given conditions, accumulations of the charges in the insulation takes ~1hr, as shown in Figure 5.12, and after this time the total accumulated charge remains practically constant with time.This is also refelected in the dynamic beaviour of the electric field observed in Figure 5.10.

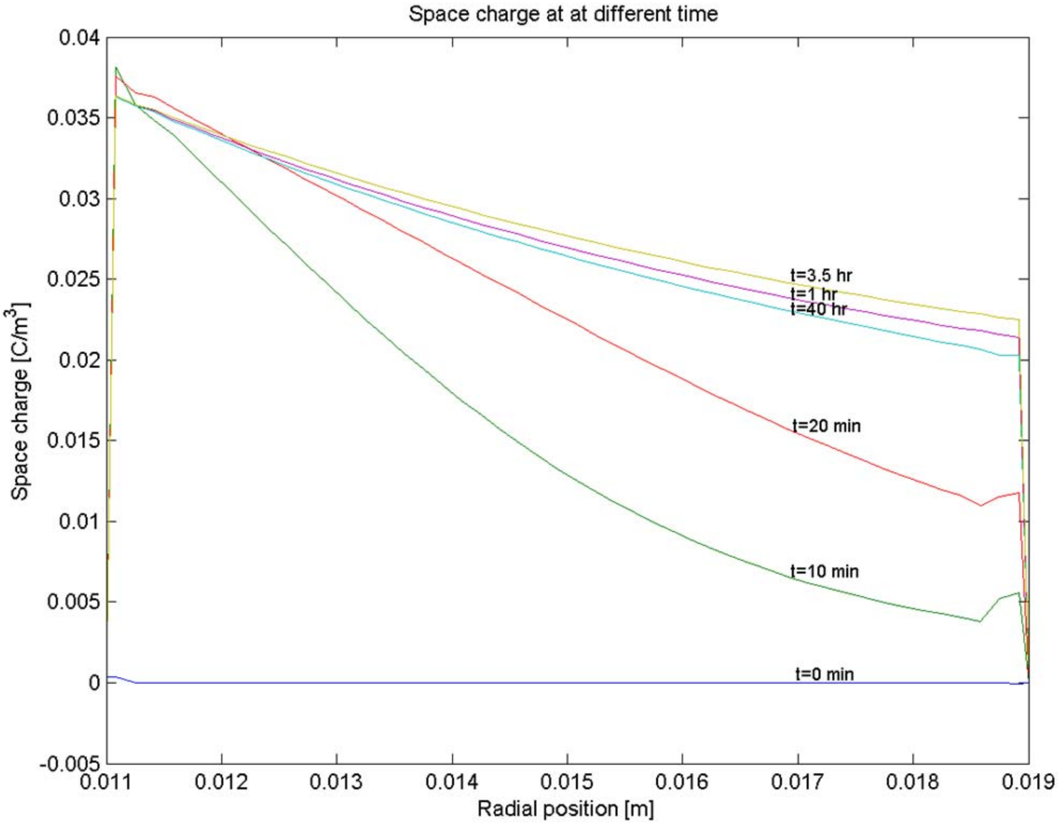

Fig.5.11: Space charge distribution across the insulation at different time

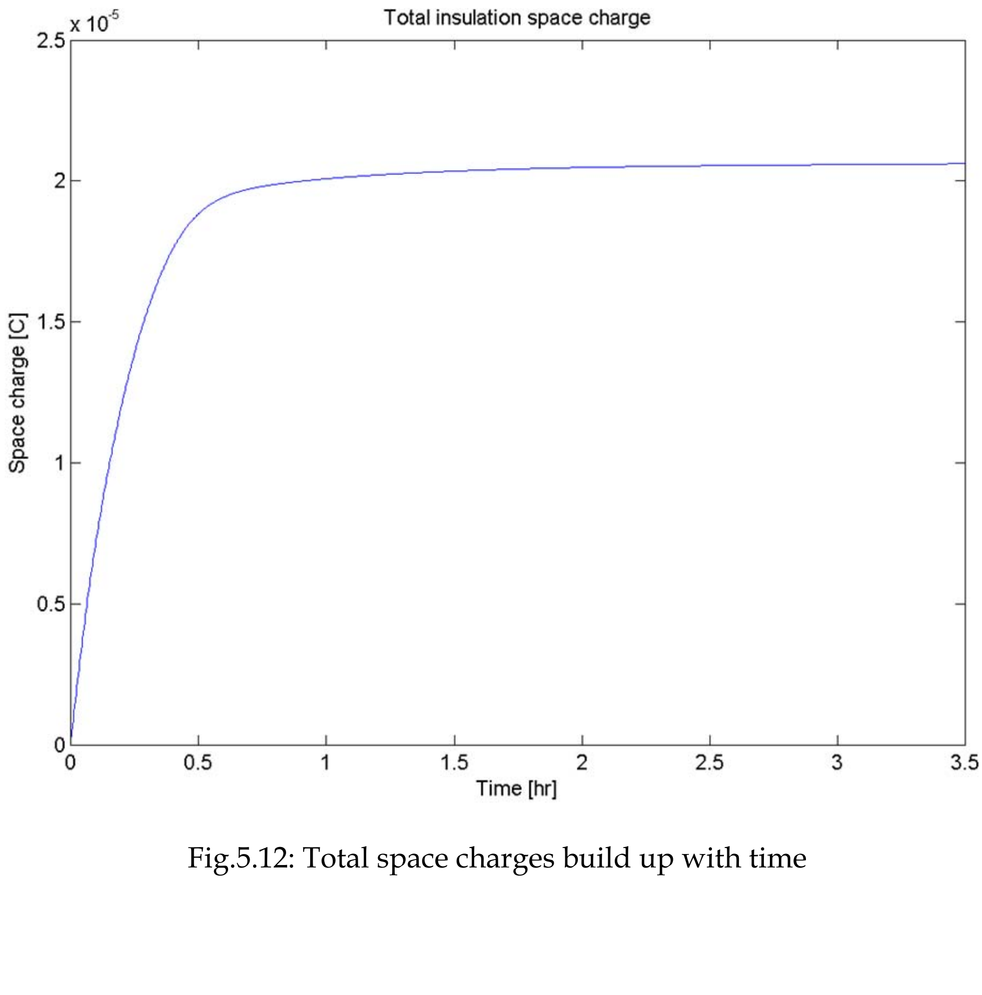

Fig.5.12: Total space charges build up with time

Chapter 6

Conclusion and Future Work

6.1 Conclusion

This thesis provides a report on the research done on the coupled electrical and thermal effects within the XLPE insulation of a HVDC power cable. An efficient computer program implementing finite volume method was developed in order to solve the steady state and transient nonlinear field problems. The MATLAB code was verified against a COMSOL model.

The developed computer program was applied to study dynamics of the temperature and electric field inversion across the insulation as well as space charges builds up with time.

6.2 Future work

Based on the experience and lessons learnt in the present study, the following future activities are proposed.

- The electrical conductivity presented in this thesis work is only a function of electric field and temperature. This is often not true in reality. The electrical conductivity is also dependent on the local composition. The composition of the insulation material is due to diffusion of various substances. Experimental measurements of a composition can be added to the developed model.
- The temperature dependency of specific heat capacity and thermal conductivity is neglected in this study. This can be added according to laboratory measurements of different materials.
- Dynamic behavior of space charge and space charge generation in polymers, which is associated with injection and trapping, is open for future works.

Bibliography

[1] D. W. V.Hartmann, "Application of HVDC for large power system interconnections," no. Cigre, pp. 1-11, 2004.

[2] C. O. Olsson, "Numerical Investigation of Temperature and Electric Field Dynamics in Polymer Insulation at HVDC," in *IEEE Electrical Insulation Conference*, Montreal, QC, Canada, May - 3 June 2009.

[3] S. Q. a. S. Boggs, "Design considerations for high voltage DC components," *IEEE Electrical Insulation Magazine,* vol. 28, no. 6, pp. 36 - 44 , Dec 2012.

[4] D. D. J. H. J. H. a. M. H. Steven Boggs, "Effect of Insulation Properties on the Field Grading of Solid Dielectric DC Cable," *IEEE Transactions on Power Delivery,* vol. 16, pp. 456-461, October 2001.

[5] J. Kuang, "Finite Element Analysis of Transient Nonlinear Coupled Field Problems," Toronto , 2000.

[6] V. W.Breuer, "Application of HVDC for large power system interconnections," no. Cigre, pp. 1-11, 2004.

[7] R. Adapa, "HVDC Technology: The State of the Art," *IEEE Power & Energy Magazine,* vol. 10, pp. 18-19, Nov/Dec 2012.

[8] Roadmap to the Supergrid Technologies, Technological, Document prepared by FOSG WG 2, March 2012.

[9] A. L. M. E. M. Allam, "Design of an optimized 600 kV DC cable system," *IEEE Transactions on Power Apparatus and Systems,* p. 1713, Sept/Oct 1980.

[10] R. Mardiana, "Parameters Affecting the Ampacity of HVDC Submarine Power Cables," *2nd International Conference on Electric Power and Energy Conversion Systems (EPECS),* pp. 1-6, 15-17 Nov 2011.

[11] M. a. P.H.F.Morshuis, "Electric fields in HVDC Paper-Insulated Cables," *IEEE Transaction on Dielctric and Insulation,* vol. 5 No.2, pp. 225-236, April 1998.

[12] T. Worzyk, Submarine Power Cables, Karlskrona: Springer Dordrecht heidelberg London New York, 2009.

[13] K. R.Bartnikas, Power and communication cables theory and applications, New York: McGraw Hill, 2000.

[14] F. H. Kreuger, Industrial High Voltage, vol. II, Delft: Delft University Press, 1995, pp. 5-34.

[15] D. C. a. I. Carstea, "Simulation of Coupled Electric and Thermal Fields in Coaxial Cables," in *6th International Conference on Telecommunications in Modern Satellite, Cable and Broadcasting Service*, Serbia and Montenegro, 2003.

[16] Y. A. a. A. J.Ghajar, Heat and mass transfer fundamentals and application, 4th Edition in SI units ed., New York: McGraw-Hill, 2011.

[17] R. J.Leveque, Finite Volume Methods for Hyperbolic Problems, second ed., The Edinburgh Building, Cambridge CB2 2RU: University of Cambridge, 2004.

[18] H. K. V. a. W. Malalasekera, An Introduction to Computational Fluid Dynamics: The Finite Volume Method, Second ed., Pearson Education Limited, 2007.

[19] G. J.Anders, Rating of electric power cables in unfavorable thermal environment, John Wiley & Sons, Inc., Hoboken, New Jersey , 2005.

[20] C. O. Olsson, "Diffusion in polymers with temperature dependent properties," *13th Int. Heat Transfer Conf.,* Aug.13-18 2006.

[21] P. L. Davidson, "Numerical Methods for Heat Diffusion," Gothenburg, Sweden, 2012.

Appendix

Multiplying both sides of Eq. (3.2) by r:

$$\frac{\partial}{\partial \mathrm{r}}\left(\mathrm{r}\sigma\frac{\partial \mathrm{V}}{\partial \mathrm{r}}\right)+\frac{\partial}{\partial t}\left[\frac{\partial}{\partial \mathrm{r}}(\mathrm{r}\varepsilon_0\varepsilon_\mathrm{r}\frac{\partial \mathrm{V}}{\partial \mathrm{r}})\right]=0 \qquad (A.1)$$

$$\mathrm{r}\rho_\mathrm{m}\mathrm{C_p}\frac{\partial T}{\partial t}=\frac{\partial}{\partial \mathrm{r}}\left(\mathrm{rk}\frac{\partial \mathrm{T}}{\partial \mathrm{r}}\right)+\ \mathrm{rS_{heat}} \qquad (A.2)$$

Integrating Eq. (A.1) and Eq.(A.2) from west to east:

$$\int_\mathrm{w}^\mathrm{e}\frac{\partial}{\partial \mathrm{r}}\left(\mathrm{r}\sigma\frac{\partial \mathrm{V}}{\partial \mathrm{r}}\right)\mathrm{dr}+\frac{\partial}{\partial t}\left[\int_\mathrm{w}^\mathrm{e}\frac{\partial}{\partial \mathrm{r}}(\mathrm{r}\varepsilon_0\varepsilon_\mathrm{r}\frac{\partial \mathrm{V}}{\partial \mathrm{r}})\mathrm{dr}\right]=0 \qquad (A.3)$$

$$\int_\mathrm{w}^\mathrm{e}\mathrm{r}\rho_\mathrm{m}\mathrm{C_p}\frac{\partial T}{\partial t}\mathrm{dr}=\int_\mathrm{w}^\mathrm{e}\frac{\partial}{\partial \mathrm{r}}\left(\mathrm{rk}\frac{\partial \mathrm{T}}{\partial \mathrm{r}}\right)\mathrm{dr}+\int_\mathrm{w}^\mathrm{e}\mathrm{rS_{heat}dr} \qquad (A.4)$$

Simplifying Eq.(A.3) and Eq.(A.4):

$$\left(\mathrm{r}\sigma\frac{\partial \mathrm{V}}{\partial \mathrm{r}}\right)_\mathrm{e}-\left(\mathrm{r}\sigma\frac{\partial \mathrm{V}}{\partial \mathrm{r}}\right)_\mathrm{w}+\frac{\partial}{\partial t}\left[\left(\mathrm{r}\varepsilon_0\varepsilon_\mathrm{r}\frac{\partial \mathrm{V}}{\partial \mathrm{r}}\right)_\mathrm{e}-\left(\mathrm{r}\varepsilon_0\varepsilon_\mathrm{r}\frac{\partial \mathrm{V}}{\partial \mathrm{r}}\right)_\mathrm{w}\right]=0 \qquad (A.5)$$

$$\frac{1}{2}(\mathrm{r_e}^2-\mathrm{r_w}^2)\rho_\mathrm{m}\mathrm{C_p}\frac{\partial T}{\partial t}=\left(\mathrm{rk}\frac{\partial \mathrm{T}}{\partial \mathrm{r}}\right)_\mathrm{e}-\left(\mathrm{rk}\frac{\partial \mathrm{T}}{\partial \mathrm{r}}\right)_\mathrm{w}+\frac{1}{2}(\mathrm{r_e}^2-\mathrm{r_w}^2)\mathrm{S_{heat}} \qquad (A.6)$$

Applying central difference scheme:

$$\left(\frac{\partial \mathrm{V}}{\partial \mathrm{r}}\right)_\mathrm{e}=\left(\frac{\mathrm{V_E}-\mathrm{V_P}}{\delta \mathrm{r_{PE}}}\right) \qquad (A.7)$$

$$\left(\frac{\partial \mathrm{V}}{\partial \mathrm{r}}\right)_\mathrm{w}=\left(\frac{\mathrm{V_P}-\mathrm{V_W}}{\delta \mathrm{r_{WP}}}\right) \qquad (A.8)$$

$$\left(\frac{\partial \mathrm{T}}{\partial \mathrm{r}}\right)_\mathrm{e}=\left(\frac{\mathrm{T_E}-\mathrm{T_P}}{\delta \mathrm{r_{PE}}}\right) \qquad (A.9)$$

$$\left(\frac{\partial T}{\partial r}\right)_w = \left(\frac{T_P - T_W}{\delta r_{WP}}\right) \tag{A.10}$$

Substituting Eq (A.7) and Eq (A.8) in to Eq (A.5) and substituing Eq (A.9) and Eq (A.10) in to Eq (A.6) gives:

$$(r\sigma)_e\left(\frac{V_E - V_P}{\delta r_{PE}}\right) - (r\sigma)_w\left(\frac{V_P - V_W}{\delta r_{WP}}\right) + \frac{\partial}{\partial t}\left[(r\varepsilon_0\varepsilon_r)_e\left(\frac{V_E - V_P}{\delta r_{PE}}\right)_e - (r\varepsilon_0\varepsilon_r)_w\left(\frac{V_P - V_W}{\delta r_{WP}}\right)\right] = 0 \tag{A.11}$$

$$\frac{1}{2}({r_e}^2 - {r_w}^2)\rho_m C_p \frac{\partial T}{\partial t} = (rk)_e\left(\frac{T_E - T_P}{\delta r_{PE}}\right) - (rk)_w\left(\frac{T_P - T_W}{\delta r_{WP}}\right) + \frac{1}{2}S_{heat}({r_e}^2 - {r_w}^2) \tag{A.12}$$

Rearanging Eq (A.11) and Eq (A.12) :

$$\left(\frac{r_e\sigma_e}{\delta r_{PE}}\right)V_E + \left(\frac{r_w\sigma_w}{\delta r_{WP}}\right)V_W - \left(\frac{r_e\sigma_e}{\delta r_{PE}} + \frac{r_w\sigma_w}{\delta r_{WP}}\right)V_P + \frac{\partial}{\partial t}\left[\left(\frac{r_e\varepsilon_0\varepsilon_r}{\delta r_{PE}}\right)V_E + \left(\frac{r_w\varepsilon_0\varepsilon_r}{\delta r_{WP}}\right)V_W - \left(\frac{r_e\varepsilon_0\varepsilon_r}{\delta r_{PE}} + \frac{r_w\varepsilon_0\varepsilon_r}{\delta r_{WP}}\right)V_P\right] = 0 \tag{A.13}$$

$$\frac{1}{2}({r_e}^2 - {r_w}^2)\rho_m C_p \frac{\partial T}{\partial t} = \left(\frac{r_e k_e}{\delta r_{PE}}\right)T_E + \left(\frac{r_w k_w}{\delta r_{WP}}\right)T_W - \left(\frac{r_e k_e}{\delta r_{PE}} + \frac{r_w k_w}{\delta r_{WP}}\right)T_P + \frac{1}{2}S_{heat}({r_e}^2 - {r_w}^2) \tag{A.14}$$

Eq (A.13) and Eq (A.14) can be writen as:

$$a_{EV1}V_E + a_{wV1}V_W - a_{PV1}V_P + \frac{\partial}{\partial t}[a_{EV2}V_E + a_{WV2}V_W - a_{PV2}V_P] = 0 \tag{A.15}$$

$$\frac{1}{2}({r_e}^2 - {r_w}^2)\rho_m C_p \frac{\partial T}{\partial t} = a_{ET1}\, T_E + a_{WT1}\, T_W - a_{PT1}\, T_P + \frac{1}{2} S_{heat}({r_e}^2 - {r_w}^2) \tag{A.16}$$

Where the coefficients are discribed below:

$$a_{EV1} = \frac{r_e \sigma_e}{\delta r_{PE}} \tag{A.17}$$

$$a_{EV2} = \frac{r_e \varepsilon_0 \varepsilon_r}{\delta r_{PE}} \tag{A.18}$$

$$a_{WV1} = \frac{r_w \sigma_w}{\delta r_{WP}} \tag{A.19}$$

$$a_{WV2} = \frac{r_w \varepsilon_0 \varepsilon_r}{\delta r_{WP}} \tag{A.20}$$

$$a_{PV1} = a_{EV1} + a_{WV1} = \frac{r_e \sigma_e}{\delta r_{PE}} + \frac{r_w \sigma_w}{\delta r_{WP}} \tag{A.21}$$

$$a_{PV2} = a_{EV2} + a_{WV2} = \frac{r_e \varepsilon_0 \varepsilon_r}{\delta r_{PE}} + \frac{r_w \varepsilon_0 \varepsilon_r}{\delta r_{WP}} \tag{A.22}$$

$$a_{ET1} = \frac{r_e k_e}{\delta r_{PE}} \tag{A.23}$$

$$a_{WT1} = \frac{r_w k_w}{\delta r_{WP}} \tag{A.24}$$

$$a_{PT1} = a_{ET1} + a_{WT1} = \frac{r_e k_e}{\delta r_{PE}} + \frac{r_w k_w}{\delta r_{WP}} \tag{A.25}$$

Taking the time integration of Eq (A.15) and Eq (A.16)

$$\int_{t}^{t+\Delta t} a_{EV1}V_E\,dt + \int_{t}^{t+\Delta t} a_{WV1}V_W\,dt - \int_{t}^{t+\Delta t} a_{PV1}V_P\,dt + \int_{t}^{t+\Delta t} \frac{\partial}{\partial t}[a_{EV2}V_E + a_{WV2}V_W - a_{PV2}V_P]dt = 0 \tag{A.26}$$

$$\int_{t}^{t+\Delta t} \frac{1}{2}(r_e{}^2 - r_w{}^2)\rho_m C_p \frac{\partial T}{\partial t}dt = \int_{t}^{t+\Delta t} a_{ET1}\,T_E dt + \int_{t}^{t+\Delta t} a_{WT1}\,T_W dt - \int_{t}^{t+\Delta t} a_{PT1}\,T_P dt + \int_{t}^{t+\Delta t} \frac{1}{2}S_{heat}(r_e{}^2 - r_w{}^2)dt \tag{A.27}$$

To evaluate the integrals of Eq. (A.26) and Eq. (A.27) an assumption is made about the variation of V_E ,V_W , V_P and T_E ,T_W , T_P with time . One may use potential/ temperatures at time t or at time $t + \Delta t$ to calculate the time integrals, or alternatively the combination of the potential /temperatures at times t and $t + \Delta t$. We can generalize this approach by introducing of a weighting parameter θ ranging between 0 and 1 and write the integral for voltage and temperature I_V and I_T with respect to time as:

$$I_V = \int_{t}^{t+\Delta t} V_P\,dt = \left[\theta V_P + (1-\theta)\,V_P{}^0\right]\Delta t \tag{A.28}$$

$$I_T = \int_{t}^{t+\Delta t} T_P\,dt = \left[\theta T_P + (1-\theta)\,T_P{}^0\right]\Delta t \tag{A.29}$$

Hence,

θ	0	1/2	1
I_V	$V_P{}^0\Delta t$	$\frac{1}{2}\left(V_P + V_P{}^0\right)$	$V_P\Delta t$
I_T	$T_P{}^0\Delta t$	$\frac{1}{2}\left(T_P + T_P{}^0\right)$	$T_P\Delta t$

If $\theta = 0$ the potential/temperature at old time level t is used. If $\theta = 1$ the potential/temperature at new time level t is used t + Δt is used; and finally if $\theta = 1/2$ the potential/temperature at t and t + Δt are equally weighted.

Therefore, using Eq (A.28) for V_E ,V_W and substituting in to Eq (A.26)

$$\begin{aligned} a_{EV1}(\theta V_E + (1-\theta) V_E{}^0)\Delta t + a_{wV1}(\theta V_W + (1-\theta) V_W{}^0)\Delta t - a_{PV1}(\theta V_P + (1-\theta) V_P{}^0)\Delta t \\ + a_{EV2}(V_E - V_E{}^0) + a_{WV2}(V_W - V_W{}^0) - a_{PV2}(V_P - V_P{}^0) = 0 \end{aligned} \tag{A.30}$$

Further, using Eq (A.29) for T_E ,T_W and substituting in to Eq (A.27)

$$\begin{aligned} &\frac{1}{2}(r_e{}^2 - r_w{}^2)\rho_m C_p(T_P - T_P{}^0) \\ &\quad = a_{ET1}\left(\theta T_E + (1-\theta) T_E{}^0\right)\Delta t + a_{WT1}\left(\theta T_W + (1-\theta) T_W{}^0\right)\Delta t \\ &\quad - a_{PT1}\left(\theta T_P + (1-\theta) T_P{}^0\right)\Delta t + \frac{1}{2}S_{heat}(r_e{}^2 - r_w{}^2)\Delta t \end{aligned} \tag{A.31}$$

Since, Crank- Nicolson scheme is used, $\theta = 1/2$. Therefore simplyfing Eq (A.30) and Eq (A.31) :

$$\begin{aligned} a_{EV1}\left(\frac{V_E + V_E{}^0}{2}\right)\Delta t + a_{wV1}\left(\frac{V_W + V_W{}^0}{2}\right)\Delta t - a_{PV1}\left(\frac{V_P + V_P{}^0}{2}\right)\Delta t + a_{EV2}(V_E - V_E{}^0) \\ + a_{WV2}(V_W - V_W{}^0) - a_{PV2}(V_P - V_P{}^0) = 0 \end{aligned} \tag{A.32}$$

$$\begin{aligned} &\frac{1}{2}(r_e{}^2 - r_w{}^2)\rho_m C_p(T_P - T_P{}^0) \\ &\quad = a_{ET1}\left(\frac{T_E + T_E{}^0}{2}\right)\Delta t + a_{WT1}\left(\frac{T_W + T_W{}^0}{2}\right)\Delta t - a_{PT1}\left(\frac{T_P + T_P{}^0}{2}\right)\Delta t \\ &\quad + \frac{1}{2}S_{heat}(r_e{}^2 - r_w{}^2)\Delta t \end{aligned} \tag{A.33}$$

Rearanging Eq (A.32) and Eq (A2.33) :

$$\begin{aligned} &\left(\frac{a_{PV1}\Delta t}{2} + a_{PV2}\right) V_P \\ &\quad = V_E\left(\frac{a_{EV1}\Delta t}{2} + a_{EV2}\right) + V_W\left(\frac{a_{WV1}\Delta t}{2} + a_{WV2}\right) + V_E{}^0\left(\frac{a_{EV1}\Delta t}{2} - a_{EV2}\right) \\ &\quad + V_W{}^0\left(\frac{a_{WV1}\Delta t}{2} - a_{WV2}\right) + \left(a_{PV2} - \frac{a_{PV1}\Delta t}{2}\right) V_P{}^0 \end{aligned} \tag{A.34}$$

$$\begin{aligned} &\left(\frac{1}{2}(r_e{}^2 - r_w{}^2)\rho_m C_p + \frac{a_{PT1}\Delta t}{2}\right) T_P \\ &\quad = a_{ET1}\left(\frac{T_E + T_E{}^0}{2}\right)\Delta t + a_{WT1}\left(\frac{T_W + T_W{}^0}{2}\right)\Delta t \\ &\quad + \left(\frac{1}{2}(r_e{}^2 - r_w{}^2)\rho_m C_p - \frac{a_{PT1}\Delta t}{2}\right) T_P{}^0 + \frac{1}{2}S_{heat}(r_e{}^2 - r_w{}^2)\Delta t \end{aligned} \tag{A.35}$$

Eq (A.34) can be written as:

$$V_P = \frac{a_{EV}V_E + a_{WV}V_W + a_{EV0}V_E{}^0 + a_{WV0}V_W{}^0 + a_{PV0}\, V_P{}^0}{a_{PV}} \tag{A.36}$$

Here:

$$a_{PV} = \frac{a_{PV1}\Delta t}{2} + a_{PV2} = \frac{\Delta t}{2}\left(\frac{r_e\sigma_e}{\delta r_{PE}} + \frac{r_w\sigma_w}{\delta r_{WP}}\right) + \left(\frac{r_e\varepsilon_0\varepsilon_r}{\delta r_{PE}} + \frac{r_w\varepsilon_0\varepsilon_r}{\delta r_{WP}}\right) \tag{A.37}$$

$$a_{EV} = \frac{a_{EV1}\Delta t}{2} + a_{EV2} = \frac{\Delta t}{2}\left(\frac{r_e\sigma_e}{\delta r_{PE}}\right) + \left(\frac{r_e\varepsilon_0\varepsilon_r}{\delta r_{PE}}\right) \tag{A.38}$$

$$a_{WV} = \frac{a_{WV1}\Delta t}{2} + a_{WV2} = \frac{\Delta t}{2}\left(\frac{r_w\sigma_w}{\delta r_{WP}}\right) + \left(\frac{r_w\varepsilon_0\varepsilon_r}{\delta r_{WP}}\right) \tag{A.39}$$

$$a_{EV0} = \frac{a_{EV1}\Delta t}{2} - a_{EV2} = \frac{\Delta t}{2}\left(\frac{r_e\sigma_e}{\delta r_{PE}}\right) - \left(\frac{r_e\varepsilon_0\varepsilon_r}{\delta r_{PE}}\right) \tag{A.40}$$

$$a_{WV0} = \frac{a_{WV1}\Delta t}{2} - a_{WV2} = \frac{\Delta t}{2}\left(\frac{r_w\sigma_w}{\delta r_{WP}}\right) - \left(\frac{r_w\varepsilon_0\varepsilon_r}{\delta r_{WP}}\right) \tag{A.41}$$

$$a_{PV0} = a_{PV2} - \frac{a_{PV1}\Delta t}{2} = \left(\frac{r_e\varepsilon_0\varepsilon_r}{\delta r_{PE}} + \frac{r_w\varepsilon_0\varepsilon_r}{\delta r_{WP}}\right) - \frac{\Delta t}{2}\left(\frac{r_e\sigma_e}{\delta r_{PE}} + \frac{r_w\sigma_w}{\delta r_{WP}}\right) \tag{A.42}$$

Eq (A.35) can be writtten as:

$$\begin{aligned}\frac{1}{2}\left(\frac{(r_e{}^2 - r_w{}^2)\rho_m C_p}{\Delta t} + a_{PT1}\right)T_P \\ = a_{ET1}\left(\frac{T_E + T_E{}^0}{2}\right) + a_{WT1}\left(\frac{T_W + T_W{}^0}{2}\right) + \frac{1}{2}\left(\frac{(r_e{}^2 - r_w{}^2)\rho_m C_p}{\Delta t} - a_{PT1}\right)T_P{}^0 \\ + \frac{1}{2}S_{heat}(r_e{}^2 - r_w{}^2)\end{aligned} \tag{A.43}$$

Rearanging Eq (A.43):

$$\left(\frac{(r_e{}^2 - r_w{}^2)\rho_m C_p}{\Delta t} + a_{PT1}\right) T_P$$
$$= a_{ET1} T_E + a_{WT1} T_W + a_{ET1} T_E{}^0 + a_{WT1} T_W{}^0 + \left(\frac{(r_e{}^2 - r_w{}^2)\rho_m C_p}{\Delta t} - a_{PT1}\right) T_P{}^0 + S_{heat}(r_e{}^2 - r_w{}^2) \quad \text{(A.44)}$$

Eq (A.44) can be written as:

$$T_P = \frac{a_{ET} T_E + a_{WT} T_W + a_{ET0} T_E{}^0 + a_{WT0} T_W{}^0 + a_{PT0} T_P{}^0 + S}{a_{PT}} \quad \text{(A.45)}$$

Here:

$$a_{PT} = \frac{(r_e{}^2 - r_w{}^2)\rho_m C_p}{\Delta t} + a_{PT1} = \frac{(r_e{}^2 - r_w{}^2)\rho_m C_p}{\Delta t} + \frac{r_e k_e}{\delta r_{PE}} + \frac{r_w k_w}{\delta r_{WP}} \quad \text{(A.46)}$$

$$a_{ET} = a_{ET1} = \frac{r_e k_e}{\delta r_{PE}} \quad \text{(A.47)}$$

$$a_{WT} = a_{WT1} = \frac{r_w k_w}{\delta r_{WP}} \quad \text{(A.48)}$$

$$a_{ET0} = a_{ET1} = \frac{r_e k_e}{\delta r_{PE}} \quad \text{(A.49)}$$

$$a_{WT0} = a_{WT1} = \frac{r_w k_w}{\delta r_{WP}} \quad \text{(A.50)}$$

$$a_{PT0} = \frac{(r_e{}^2 - r_w{}^2)\rho_m C_p}{\Delta t} - a_{PT1} = \frac{(r_e{}^2 - r_w{}^2)\rho_m C_p}{\Delta t} - \left(\frac{r_e k_e}{\delta r_{PE}} + \frac{r_w k_w}{\delta r_{WP}}\right) \quad \text{(A.51)}$$

$$S = S_{heat}(r_e{}^2 - r_w{}^2) \quad \text{(A.52)}$$

Therefore Eq. (A.36) and Eq. (A.45) are iteratively solved using Gauss Sedial method.